Chapter 3
Various Electromagnetic Phenomena

3.1 Geometrical Effect

In the last chapter the magnetization and AC loss in a wide superconducting slab were calculated. In this section we discuss the electromagnetic phenomena in a superconductor with other geometries. The cases are treated where the current, the transverse AC field or the transverse rotating field is applied to a cylindrical superconductor.

3.1.1 Loss in Superconducting Wire due to AC Current

We assume that AC current is applied to a straight superconducting cylinder of radius R without external magnetic field. In this case only the self field in the azimuthal direction exists. If the magnitude of the AC current is denoted by $I(t)$, the value of the self field at the surface, $r = R$, is given by

$$H_{\mathrm{I}} = \frac{I}{2\pi R}. \tag{3.1}$$

The penetration of the azimuthal flux lines due to the self field is also described by the critical state model as in Sect. 2.5. We assume again the Irie-Yamafuji model [1] given by (2.46) for the magnetic field dependence of the pinning force density. The azimuthal magnetic flux density and its magnitude are represented by B and $\widehat{B}$, respectively. The force balance equation in the quasistatic process is described as

$$-\frac{\widehat{B}}{\mu_0 r} \cdot \frac{\mathrm{d}}{\mathrm{d}r}(r\widehat{B}) = \delta \alpha_{\mathrm{c}} \widehat{B}^{\gamma}, \tag{3.2}$$

where δ is a sign factor indicating the direction of the flux motion, e.g. $\delta = 1$ indicates that flux lines move in the radial direction. Equation (3.2) can be easily solved

T. Matsushita, *Flux Pinning in Superconductors*,
Springer Series in Solid-State Sciences 178,
DOI 10.1007/978-3-642-45312-0_3, © Springer-Verlag Berlin Heidelberg 2014

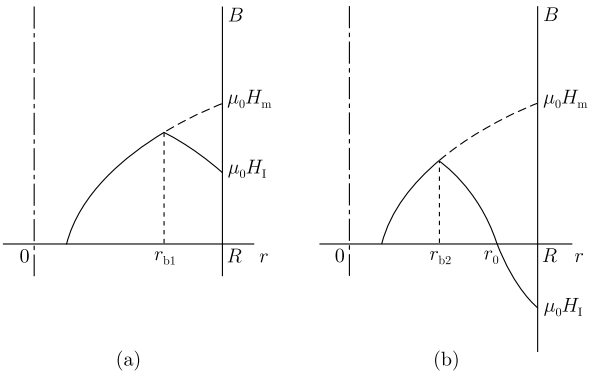

Fig. 3.1 Distribution of azimuthal magnetic flux in a superconducting cylinder while the self field due to the AC current changes from H_m to $-H_m$. (**a**) and (**b**) correspond to cases where the current flows in the positive and negative z-axis directions, respectively

yielding for the magnetic flux distribution:

$$\delta(r\widehat{B})^{2-\gamma} = \delta_R(R\mu_0\widehat{H_I})^{2-\gamma} + \frac{2-\gamma}{3-\gamma}\alpha_c\mu_0\left(R^{3-\gamma} - r^{3-\gamma}\right), \tag{3.3}$$

where $\widehat{H_I} = |H_I|$, and δ_R is the value of δ at the surface ($r = R$), and the boundary condition

$$B(r = R) = \mu_0 H_I \tag{3.4}$$

was used.

The energy loss can be calculated from (2.74) as was done previously. But we calculate it more easily in terms of Poynting's vector. Since the induced electric field $\boldsymbol{E}$ and the magnetic flux density $\boldsymbol{B}$ are expressed as $(0, 0, E)$ and $(0, B, 0)$ from symmetry, Poynting's vector, $(\boldsymbol{E} \times \boldsymbol{B})/\mu_0$, at the surface is directed negative radially, and hence, towards the inside of the superconductor. Then, the energy loss density per cycle of the AC current is written as

$$\begin{aligned} W &= \frac{2}{R\mu_0}\int \mathrm{d}t\, E(R,t)B(R,t) \\ &= \frac{2}{R\mu_0}\int \mathrm{d}t\, B(R,t)\int_0^R \frac{\partial}{\partial t}B(r,t)\mathrm{d}r, \end{aligned} \tag{3.5}$$

where the integral with respect to time is carried out for the period of one cycle. From symmetry we have only to double the contribution from the period in which the current varies from the maximum value, I_m, to $-I_m$. If the maximum self field is denoted by $H_m = I_m/2\pi R$, this half cycle is divided into the periods (i) and (ii) in which H_I changes from H_m to 0 and from 0 to $-H_m$ as shown in Fig. 3.1(a) and 3.1(b), respectively. In period (i), $B > 0$ and $\delta = 1(\delta_R = 1)$ in the entire area, $r_{b1} \le r \le R$, in which the magnetic flux distribution changes. On the other hand, in period (ii), we have $\delta_R = -1$ and $B > 0$ and $\delta = 1$ for $r_{b2} \le r \le r_0$, while $B < 0$ and $\delta = -1$ for $r_0 < r \le R$. From (3.3) the critical current is given by

$$I_c = 2\pi \left(\frac{2-\gamma}{3-\gamma} \alpha_c \mu_0^{\gamma-1} R^{3-\gamma} \right)^{1/(2-\gamma)}. \tag{3.6}$$

If the corresponding self field is denoted by

$$H_{Ip} = \frac{I_c}{2\pi R}, \tag{3.7}$$

r_{b1}, r_{b2} and r_0 are respectively given by

$$1 - \left(\frac{r_{b1}}{R} \right)^{3-\gamma} = \frac{1}{2H_{Ip}^{2-\gamma}} \left(H_m^{2-\gamma} - \widehat{H}_I^{2-\gamma} \right), \tag{3.8a}$$

$$1 - \left(\frac{r_{b2}}{R} \right)^{3-\gamma} = \frac{1}{2H_{Ip}^{2-\gamma}} \left(H_m^{2-\gamma} + \widehat{H}_I^{2-\gamma} \right), \tag{3.8b}$$

$$1 - \left(\frac{r_0}{R} \right)^{3-\gamma} = \left(\frac{\widehat{H}_I}{H_{Ip}} \right)^{2-\gamma}. \tag{3.8c}$$

Since the variation in the magnetic flux distribution with respect to time comes only from the variation in H_I, (3.5) reduces to

$$\begin{aligned} W = 4\mu_0 H_{Ip}^2 \int_0^{h_m} \mathrm{d}h_I h_I^{2-\gamma} \Bigg[& - \int_{x_1}^1 \frac{\mathrm{d}x}{x} \left(1 + h_I^{2-\gamma} - x^{3-\gamma} \right)^{(\gamma-1)/(2-\gamma)} \\ & + \int_{x_2}^{x_0} \frac{\mathrm{d}x}{x} \left(1 - h_I^{2-\gamma} - x^{3-\gamma} \right)^{(\gamma-1)/(2-\gamma)} \\ & + \int_{x_0}^1 \frac{\mathrm{d}x}{x} \left(x^{3-\gamma} - 1 + h_I^{2-\gamma} \right)^{(\gamma-1)/(2-\gamma)} \Bigg], \end{aligned} \tag{3.9}$$

where

$$h_m = \frac{H_m}{H_{Ip}}, \qquad h_I = \frac{\widehat{H}_I}{H_{Ip}}, \tag{3.10}$$

$$x_0 = \frac{r_0}{R}, \qquad x_1 = \frac{r_{b1}}{R}, \qquad x_2 = \frac{r_{b2}}{R}. \tag{3.11}$$

An analytic calculation can be carried out only for $\gamma = 1$, yielding [2]

$$W = 4\mu_0 H_{Ip}^2 \left[h_m \left(1 - \frac{h_m}{2} \right) + (1 - h_m) \log(1 - h_m) \right]. \tag{3.12}$$

This value reduces to $W \simeq 4\mu_0 H_m^3 / \alpha_c R$ for $h_m \ll 1$ and amounts to double that value for the superconducting slab, i.e., the value given by (2.80) with $\gamma = 1$, where d is approximately replaced by R. This comes from the fact that the surface region where the energy dissipation occurs is relatively wider for the case of superconducting cylinder. The energy loss density is expressed as [3]

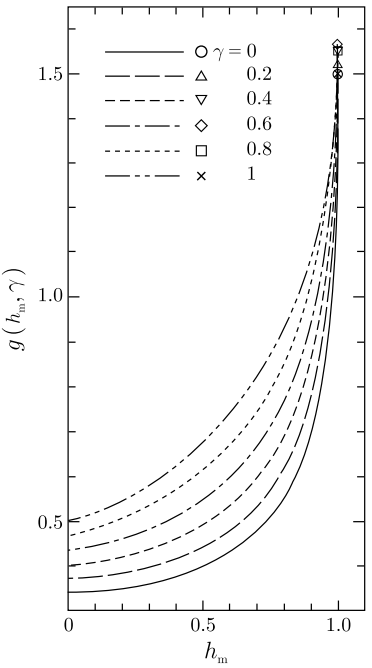

Fig. 3.2 Function $g(h_\mathrm{m}, \gamma)$

$$W = \frac{4}{3}(2-\gamma)\mu_0 g(h_\mathrm{m}, \gamma)\frac{H_\mathrm{m}^{4-\gamma}}{H_\mathrm{Ip}^{2-\gamma}} \tag{3.13}$$

analogously to (2.80), where g is given by a double integral and is a function of h_m and γ as shown in Fig. 3.2. When γ is a rational number, g can be expressed in the form of a single integral.

3.1.2 Loss in Superconducting Wire of Ellipsoidal Cross Section and Thin Strip due to AC Current

Norris [4] calculated the loss in a superconducting wire with an ellipsoidal cross section and a thin superconducting strip due to AC current using the Bean-London model ($\gamma = 1$) [5, 6]. According to the calculated result, the loss in the ellipsoidal wire of the cross sectional area S is essentially the same as that in a cylindrical wire given by (3.12). In terms of the current, it leads to

$$W = \frac{\mu_0 I_\mathrm{c}^2}{\pi S}\left[i_\mathrm{m}\left(1-\frac{i_\mathrm{m}}{2}\right)+(1-i_\mathrm{m})\log(1-i_\mathrm{m})\right] \tag{3.14}$$

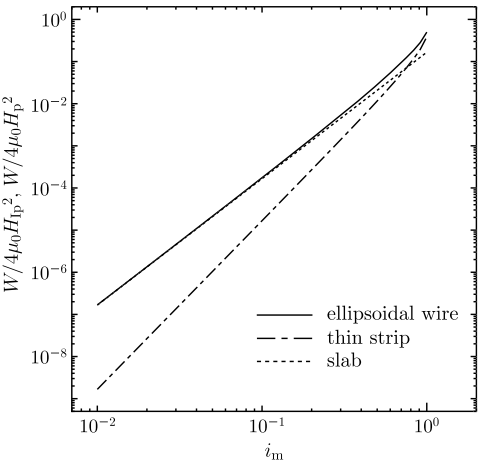

Fig. 3.3 Calculated AC current loss in superconducting ellipsoidal wire and thin strip [4] for the case of $\gamma = 1$. The *broken line* shows the loss in a superconducting slab

with the normalized current amplitude:

$$i_{\rm m} = \frac{I_{\rm m}}{I_{\rm c}}. \tag{3.15}$$

In the case of a thin superconducting strip of the cross sectional area S, the loss is given by

$$W = \frac{\mu_0 I_{\rm c}^2}{\pi S}\left[(1 - i_{\rm m})\log(1 - i_{\rm m}) + (1 + i_{\rm m})\log(1 + i_{\rm m}) - i_{\rm m}^2\right]. \tag{3.16}$$

The AC losses in the superconducting ellipsoidal wire and the thin strip are shown in Fig. 3.3. The loss in the ellipsoidal wire approaches that of the equivalent slab at small current amplitudes, while the current amplitude dependence is significantly different for the thin strip with a small loss at small current amplitudes.

3.1.3 Transverse Magnetic Field

We have treated the cases where the physical quantities depend only on one coordinate axis without being influenced by the geometrical factor such as a demagnetization factor of superconductor. In this subsection we treat the case where a transverse magnetic field is applied to a cylindrical superconductor. Because of the break in symmetry the physical quantities depend on two coordinate axes and we have to solve a two-dimensional problem.

A very small transverse magnetic field is supposed to be applied to a cylindrical superconductor. The initial state is assumed and the diamagnetism at the surface is disregarded for simplicity. The inner part of the superconductor is completely shielded and the magnetic flux density there is zero. The shielding current flows only

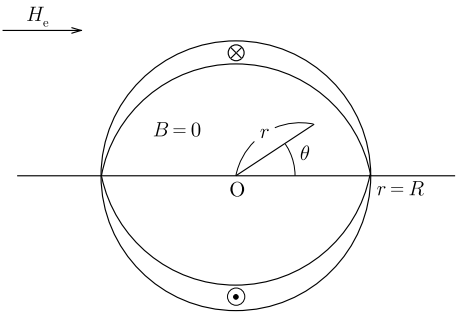

Fig. 3.4 Surface layer of shielding current in a superconducting cylinder in a small transverse magnetic field

in the vicinity of the surface. If the thickness of the region in which the shielding current flows is sufficiently small, an approximate solution can be obtained. We define the cylindrical coordinates as shown in Fig. 3.4, where H_e is the uniform external magnetic field and R is the radius of the superconductor. After applying a method well known in electromagnetism we obtain the solution:

$$\left.\begin{aligned} B_r &= \mu_0 H_e \left(1 - \frac{R^2}{r^2}\right) \cos\theta \\ B_\theta &= -\mu_0 H_e \left(1 + \frac{R^2}{r^2}\right) \sin\theta \end{aligned}\right\}; \quad r > R \tag{3.17}$$

and

$$B_r = B_\theta = 0; \quad 0 < r < R. \tag{3.18}$$

The azimuthal magnetic flux density B_θ is not continuous at $r = R$ and the current corresponding to the difference flows along the z-axis on the surface of the superconductor. If we represent this surface current density by $\tilde{J}$ (A m^{-1}), we have

$$\tilde{J}(\theta) = -2H_e \sin\theta. \tag{3.19}$$

In practice the critical current density originating from flux pinning is finite and the thickness of the shielding-current region is also finite. If we use the Bean-London model [5, 6] in which the critical current density is independent of the magnetic field, the thickness is $(2H_e/J_c)|\sin\theta|$.

When the magnetic field becomes much larger, the shielding-current region becomes wider and the completely shielded region becomes narrower as shown in Fig. 3.5. According to the critical state concept the distribution of the shielding current shown in Fig. 3.5(a) is determined so as to minimize the variation in the magnetic flux distribution inside the superconductor, i.e., to minimize the invasion of the magnetic flux. However, the analytic exact solution has not yet been obtained even for the simple Bean-London model. The detailed discussion on the magnetic flux distribution is given in [7–9]. Now the approximate schemes are used in which the region of shielding current is assumed to be of simple shape and determined

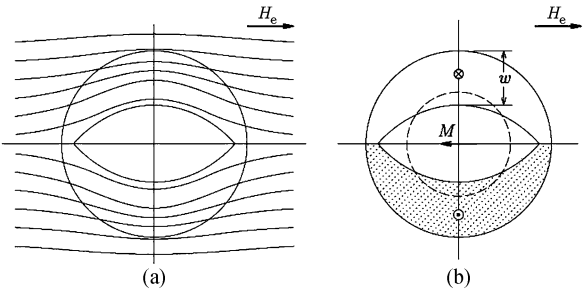

Fig. 3.5 (**a**) Magnetic structure and (**b**) shielding current distribution in a superconducting cylinder in large AC transverse magnetic field. Circular current layer shown by the *broken line* is sometimes assumed simply. M denotes the magnetization due to the shielding current

by the condition that $B = 0$ is satisfied at some special points within the shielded region. In the simplest case a shielding-current region of a circular shape is assumed as shown by the broken line in Fig. 3.5(b) and its radius is determined by the condition that $B = 0$ at the center of the cylindrical superconductor. Even such a simplified approximation [10] with the Bean-London model leads to magnetization and loss due to the transverse AC magnetic field which are rather close to the results [9] of numerical analysis. In [11] the magnetization and the loss are analyzed using the Irie-Yamafuji model [1] for the magnetic field dependence of the pinning force density, and the magnetic flux distribution is determined on the assumption that the magnitude of the shielding current density is a function only of the distance from the center of the cylinder. These calculated results are compared with experimental results in detail. According to the calculated result the AC loss in the range of small field amplitude is four times as large as (2.80) for a superconducting slab in a parallel field. This is caused by the fact that the amount of shielding current is enhanced due to the effect of demagnetization. That is, from an approximate estimate as in (2.82) the enhancement factor is calculated as the average of $(2\sin\theta)^3$ in the angular region $0 \leq \theta \leq \pi$, which is equal to $32/3\pi \simeq 3.4$. This is close to the analytical result, 4.

When the transverse AC magnetic field becomes larger than the penetration field given by

$$H_{p\perp} = \frac{1}{\mu_0}\left[\frac{2}{\pi}(2-\gamma)\mu_0\alpha_c R\right]^{1/(2-\gamma)}, \tag{3.20}$$

the shielding current extends to the entire region of the cylinder and currents of the opposite directions flow in the upper and lower halves. In this case the exact solution has not yet been obtained except for $\gamma = 1$ where the magnetic flux distribution is uniquely determined. In case $\gamma \neq 1$ an approximate solution is obtained assuming that the magnitude of the shielding current depends only on the distance from the center of cylinder. The error in the hysteresis loss obtained from this result in comparison with the numerically calculated loss is within 10 % [11] even in the vicinity of the penetration field where the error is largest. The losses obtained for various γ values are shown in Fig. 3.6.

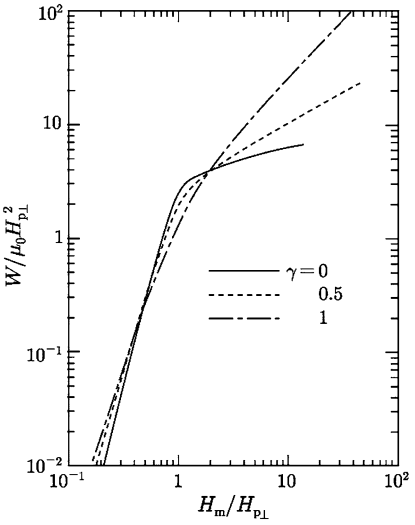

Fig. 3.6 Energy loss density in a superconducting cylinder due to AC transverse magnetic field [11]

3.1.4 Rotating Magnetic Field

We shall next consider the case where a transverse magnetic field is applied to a cylindrical superconductor and then rotated. Provided that the rotating angle is small, the rotation is almost identical to a superposition of a small magnetic field in the direction normal to the initial field. Hence, a new shielding current is induced by the superposed field. The net current distribution is obtained by superposition of the newly induced distribution upon the initial one. When the rotating angle becomes much larger, the current distribution must be obtained in a different way. Extrapolating from the distribution under the small rotating angle, the current distribution inside the superconductor in the steady state is deduced to be that shown in Fig. 3.7. Although this distribution is to be determined under the condition that $B = 0$ is satisfied throughout the entire shielded region, it cannot be generally determined correctly. In case $\gamma = 1$ where the magnitude of shielding current density is constant, a solution which satisfies $B = 0$ approximately in the shielded region can be obtained [12] only when the magnetic field is so small that the thickness of the shielding current layer is small. In case $\gamma \neq 1$ an approximate solution is obtained [12] from the requirement that $B = 0$ at the center of cylinder with the assumption that the shielding current density depends only on the distance from the center. From the shielding current distribution the magnetic flux distribution is obtained. The induced electric field $\boldsymbol{E}$ can be calculated from the variation in the magnetic flux distribution and the loss is estimated from $\boldsymbol{J} \cdot \boldsymbol{E}$. The energy loss density [12] so obtained is $8/\pi$ times as large as the loss due to the transverse AC magnetic field with the same amplitude discussed in Sect. 3.1.3, and hence, $32/\pi$ times as large as the value given by (2.80).

On the other hand, the current distribution in the steady state is shown in Fig. 3.8 where the magnetic flux penetrates up to the center in a transverse field greater than

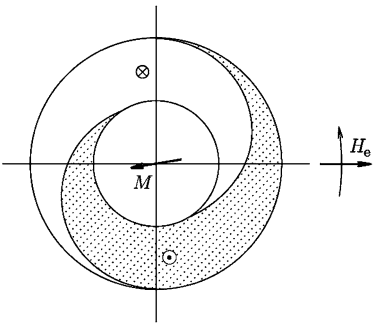

Fig. 3.7 Steady distribution of shielding current in a superconducting cylinder in a small rotating transverse magnetic field

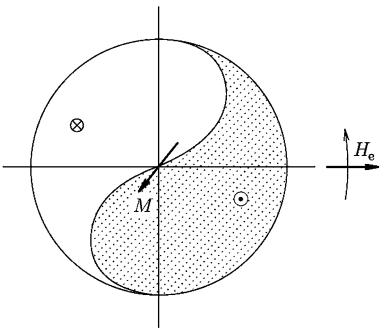

Fig. 3.8 Steady distribution of shielding current in a superconducting cylinder in a rotating transverse magnetic field of magnitude larger than the penetration field

the penetration field $H_{p\perp}$. In this case there is no region where the magnetic flux is completely shielded and the current distribution is determined using the condition that the electric field E is zero on the boundary of the two regions where the current flows are opposite to each other. This condition is based on the irreversibility in the critical state model which requires that the current and the electric field are in the same direction, i.e., $\boldsymbol{J} \cdot \boldsymbol{E} > 0$. The current distribution and the loss are calculated using the above-mentioned assumption that the current density depends only on the distance from the center [12].

In the intermediate region where the magnetic field is comparable to the penetration field, the approximate expression of the energy loss density is derived by interpolating the result in each region [12]. Agreement between this expression and the numerically calculated result [9] is obtained for case $\gamma = 1$.

3.1.5 AC Loss in a Thin Superconducting Strip in Normal Magnetic Field

The AC energy loss in a thin superconducting strip in a normal AC magnetic field was theoretically calculated by Brandt et al. [13]. They assumed that the superconducting strip is so thin that the current distribution within the thickness can be

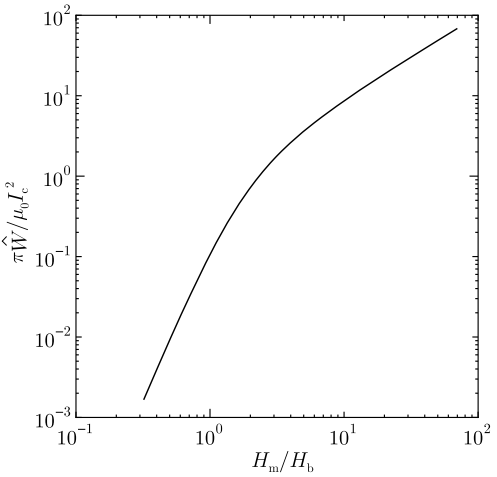

Fig. 3.9 AC energy loss density in a unit length of superconducting strip vs. normal AC magnetic field amplitude [13]

disregarded. The critical current density was assumed to be independent of the magnetic field. It is assumed that the shielding current with the critical current density penetrates from the edges of the superconductor as the magnetic field increases, similarly to the prediction of the critical state model. It is also assumed that the current flows with a smaller density, even in the interior region, to shield it from the normal magnetic field, which is different from the prediction of the critical state model for a bulk superconductor. It should be noted that there is no distinction between the surface and the interior region, since the thin limit is assumed.

Although the details of the theoretical calculation are omitted, the AC energy loss density in a unit length of the strip in one period of the normal AC magnetic field of amplitude H_m is given by

$$\widehat{W} = \frac{\mu_0 I_\mathrm{c}^2}{\pi}\left(2\log\cosh\frac{H_\mathrm{m}}{H_\mathrm{b}} - \frac{H_\mathrm{m}}{H_\mathrm{b}}\tanh\frac{H_\mathrm{m}}{H_\mathrm{b}}\right), \tag{3.21}$$

where $H_\mathrm{b} = I_\mathrm{c}/(2\pi a)$ is the characteristic field, with $2a$ and I_c denoting the strip width and critical current, respectively. Thus, we have $\widehat{W} \simeq 2\pi\mu_0 a^2 H_\mathrm{m}^4/(3H_\mathrm{b}^2)$ for $H_\mathrm{m} \ll H_\mathrm{b}$ and $\widehat{W} \simeq 4\pi\mu_0 a^2 H_\mathrm{b} H_\mathrm{m}$ for $H_\mathrm{m} \gg H_\mathrm{b}$. Hence, the AC energy loss density for small AC field amplitudes is close to the value when an AC current is applied, and that for large AC field amplitudes is close to the value when a parallel magnetic field is applied. The AC field amplitude dependence of the AC energy loss density in a unit length of the strip is shown in Fig. 3.9.

3.2 Dynamic Phenomena

We have treated only the quasistatic process in which the variation in the magnetic flux distribution is very slow. This process is not the one used in thermodynamics

but the one in which the variation in the inner magnetic flux distribution with time depends only on the time variation of the external sources such as the magnetic field. In this case the viscous force can be neglected and the magnetic flux distribution is determined from the balance between the Lorentz force and the pinning force. In this section we shall discuss the case where the external variable varies so quickly that the viscous force cannot be neglected.

For simplicity the one-dimensional problem is again treated where the external magnetic field is applied along the z-axis of a semi-infinite superconductor occupying $x \geq 0$. Since the force balance equation obtained by substitution of (2.46) into (2.13) is nonlinear, an analytic solution is not easily obtained [1]. We suppose that a small varying field is superposed on a large external magnetic field, H_e. The internal magnetic flux density is expressed as

$$B(x,t) = \mu_0 H_e + b(x,t) \tag{3.22}$$

In the above $b(x,t)$ is considered to be much smaller than $\mu_0 H_e$. If we assume that H_e is positive, B is also positive. The continuity equation for flux lines (2.15) is approximately rewritten as

$$\frac{\partial b}{\partial t} = -\mu_0 H_e \frac{\partial v}{\partial x}. \tag{3.23}$$

The force balance equation (2.13) approximately reduces to

$$H_e \frac{\partial b}{\partial t} + \delta F_p(\mu_0 H_e) + \eta \frac{\mu_0 H_e}{\phi_0} v = 0, \tag{3.24}$$

where $v = \delta \hat{v}$ is used. Derivation of this equation with respect to x and elimination of v lead to a diffusion equation for b. The breaking point, x_b, is used as one of the boundary conditions to determine the magnetic flux distribution. However, this equation cannot be easily solved, since this boundary inside the superconductor varies with time.

In this section we treat the case where the viscous force is sufficiently small that the magnetic flux distribution can be approximately obtained by an iterative calculation from a quasistatic one. For example we assume that a slowly varying sinusoidal AC magnetic field of amplitude h_0 and frequency $\omega/2\pi$ is superposed on the DC field H_e. The condition required for the frequency will be discussed later. The boundary condition at the surface is given by

$$b(0,t) = \mu_0 h_0 \cos \omega t. \tag{3.25}$$

When the viscous force can be neglected, the magnetic flux distribution is obtained from (3.24) as

$$\begin{aligned} b(x,t) &= \mu_0 (h_0 \cos \omega t - \delta J_c x) \\ &\equiv b_0(x,t); \quad 0 < x < x_{b0}, \end{aligned} \tag{3.26}$$

where $F_p(\mu_0 H_e) = \mu_0 H_e J_c$ with J_c denoting the constant critical current density, $\delta = -\operatorname{sign}(\sin \omega t)$ and

$$x_{b0} = \frac{h_0}{2J_c}(1 + \delta \cos \omega t). \tag{3.27}$$

From (3.23) and (3.26) we have

$$v = -\frac{1}{\mu_0 H_e} \int_{x_{b0}}^{x} \frac{\partial b_0}{\partial t} dx = \frac{h_0}{H_e} \omega \sin \omega t (x - x_{b0}). \tag{3.28}$$

Substitution of (3.28) into the third term in (3.24) leads to

$$b(x,t) = b_0(x,t) - \frac{\eta \mu_0 h_0 \omega}{2\phi_0 H_e} \sin \omega t \left(x^2 - 2x_{b0}x\right). \tag{3.29}$$

This solution holds in the region from the surface to the breaking point of the magnetic flux distribution x_b, which is slightly different from x_{b0} in (3.27). The new breaking point is obtained as a crossing point between the distribution given by (3.29) and the "previous" distribution. Since the distribution given by (3.29) agrees with the quasistatic distribution at $\omega t = n\pi$, with n denoting an integer at which the sign factor δ changes, the "previous" distribution is the quasistatic one. Hence, after a simple calculation we have approximately

$$x_b = x_{b0} - \frac{\eta h_0 \omega}{4\phi_0 H_e J_c} |\sin \omega t| x_{b0}^2 \tag{3.30}$$

up to the first order in ω. The second term in (3.30) should be smaller than the first so that the iterative approximation holds true. Since x_{b0} becomes as large as h_0/J_c, the condition for the frequency is written as

$$\omega \ll \frac{4\phi_0 H_e J_c^2}{\eta h_0^2} \equiv \omega_0. \tag{3.31}$$

The AC component of the magnetic flux density averaged over the superconductor in the period $0 \le \omega t \le \pi$ is to first order in ω given by

$$\langle b \rangle = \frac{\mu_0 h_0^2}{4J_c d} \left[\sin^2 \omega t + 2 \cos \omega t + \frac{2\omega}{3\omega_0} \sin \omega t (1 - \cos \omega t)^3 \right]. \tag{3.32}$$

From symmetry the energy loss density per cycle of the AC field is

$$W = 2 \int_{-h_0}^{h_0} \langle b \rangle d(h_0 \cos \omega t) = \frac{2\mu_0 h_0^3}{3J_c d} \left(1 + \frac{7\pi\omega}{16\omega_0} \right). \tag{3.33}$$

The first term is the pinning energy loss density in the quasistatic process; it agrees with the result of (2.80) after substituting $\gamma = 1$. The second term is the viscous energy loss density. The reason why the pinning energy loss density is not different

from that in the quasistatic case is that the magnetic flux distributions at $\omega t = 0$ and π are the same as those in the quasistatic case, i.e., the amount of magnetic flux which contributes to the pinning loss during one cycle is unchanged. The second term in (3.33) can also be calculated directly from the second term in (2.73) as the viscous energy loss density (see Exercise 3.2).

When the frequency of the AC magnetic field becomes higher, it is necessary to take into account terms to higher order in ω. In this case the "previous" distribution in the region where $x_b < x$ varies with time, and hence, the calculation becomes extremely complicated. According to the theoretical analysis of Kawashima et al. [14] the energy loss density in this case is predicted to be

$$W = \frac{2\mu_0 h_0^3}{3J_c d}\left[1 + \frac{7\pi\omega}{16\omega_0} - \frac{512}{105}\left(\frac{\omega}{\omega_0}\right)^2\right]. \tag{3.34}$$

The decrease in the energy loss density at high frequencies is caused by the fact that the amount of moving flux decreases due to the stronger shielding action of the viscous force.

3.3 Superposition of AC Magnetic Field

3.3.1 Rectifying Effect

When a small AC magnetic field is applied to a current-carrying superconducting wire or tape in a transverse DC field, the current-voltage characteristics vary with a decrease in the critical current density [15, 16] as shown in Fig. 3.10. Sometimes the critical current density reduces to zero. This is commonly observed independently of whether the AC field is parallel or normal to the DC field. Here we shall first argue the case of parallel AC field. The current-voltage characteristics in this case can also be analyzed in terms of a magnetic flux distribution in the superconductor as predicted by the critical state model. The magnetic flux distribution is predicted to vary with the surface field during one cycle of AC field as shown in Fig. 3.11. The arrows in the figure represent the direction of flux motion. It is seen that the flux motion is not symmetric. That is, the amount of flux that moves from the left to the right is larger than that in the opposite direction and a DC component of electric field appears due to the rectifying effect of flux flow [15]. Strictly speaking, (2.13) should be used, since a resistive state is being treated. But here, for simplicity the viscous force is disregarded. When the pinning force is strong as in a commercial superconductor, this approximation is valid within the practical range of the electric field.

We assume a superconducting slab of width $2d$ carrying a transport current of density J_t smaller than J_c. The Bean-London model ($\gamma = 1$ and $J_c = \text{const.}$) is used for the pinning force density. The net magnetic flux Φ that flows from the left to the

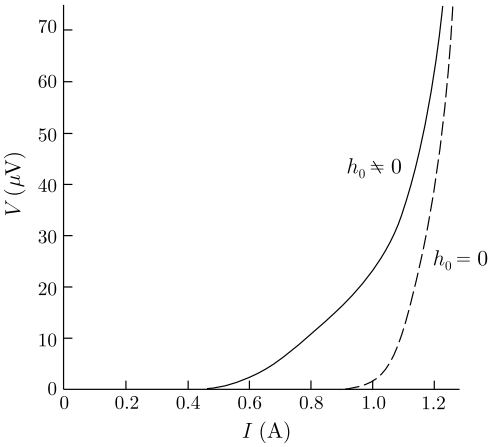

Fig. 3.10 Current-voltage characteristics in a superconducting Pb-Bi foil with (*solid line*) and without (*broken line*) superposed small AC magnetic field perpendicular to both the normal DC magnetic field and the current [16]

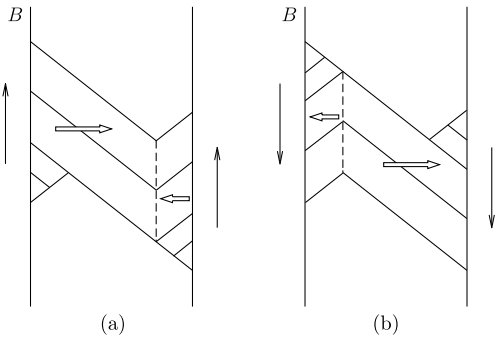

Fig. 3.11 Explanation of rectifying effect by the Kaiho model [15] in case where DC and AC magnetic fields are parallel to a superconducting slab. (**a**) and (**b**) show magnetic flux distributions in the phases of increasing and decreasing AC magnetic field, respectively

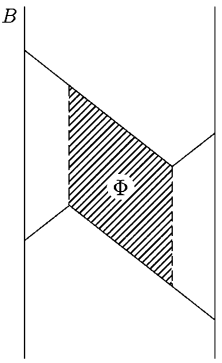

Fig. 3.12 *Shadowed region* corresponds to the magnetic flux passing through the superconducting slab during one cycle of AC magnetic field

right during one cycle of the AC field of amplitude h_0 corresponds to the area of hatched region in Fig. 3.12 and can be calculated as

$$\Phi = 4\mu_0 j\big[h_0 - H_{\mathrm{p}}(1-j)\big]d, \tag{3.35}$$

where $H_p = J_c d$ is the penetration field and $j = J_t/J_c$. Hence, the average value of the electric field is given by

$$\overline{E} = \Phi f, \tag{3.36}$$

where f is the frequency of the AC field. The apparent critical current density J_c^* is obtained from the condition $\overline{E} = 0$ as

$$J_c^* = J_c\left(1 - \frac{h_0}{H_p}\right). \tag{3.37}$$

Hence, $J_c^* = 0$ for $h_0 > H_p$.

Now we shall estimate the energy loss in the resistive state. One part of the dissipated energy is supplied by the DC current source and is given by $W_c = J_t\overline{E}/f = J_t\Phi$ per unit volume. The other part is supplied by the AC magnet and its value per unit volume is given by

$$W_f = \int \langle B\rangle \mathrm{d}H(t), \tag{3.38}$$

where $\langle B\rangle$ is the magnetic flux density averaged over the superconducting slab and $H(t)$ is the instantaneous value of the AC magnetic field. After a simple calculation we have [17]

$$W_f = 2\mu_0 H_p h_0\left(1 - j^2\right) - \frac{4}{3}\mu_0 H_p^2\left(1 - 3j^2 + 2j^3\right). \tag{3.39}$$

Thus, the total energy loss density is

$$W = W_c + W_f = 2\mu_0 H_p h_0\left(1 + j^2\right) - \frac{4}{3}\mu_0 H_p^2\left(1 - j^3\right). \tag{3.40}$$

This result can also be directly obtained from the method shown in (2.74) (verify that the two methods derive the same result, Exercise 3.3).

Secondly we shall discuss the case where the AC and DC magnetic fields are perpendicular to each other. For example, we assume that the wide superconducting slab parallel to the y-z plane carries a DC transport current along the y-axis in a DC magnetic field along the x-axis and an AC field along the z-axis. In this case the assumption that $\partial/\partial y = \partial/\partial z = 0$ seems to be allowed. The magnetic flux density has only the x- and z-components, B_x and B_z. The condition of $\nabla \cdot \boldsymbol{B} = 0$ leads to a B_x that is uniform and equal to $\mu_0 H_e$ with H_e denoting the DC magnetic field. Hence, only the component B_z varies along the x-axis and the current density along the y-axis is given by

$$J = -\frac{1}{\mu_0} \cdot \frac{\partial B_z}{\partial x}. \tag{3.41}$$

Hence, the mathematical expression is similar to the case of parallel DC and AC fields discussed above and hence the same analysis can be repeated. Thus, a similar rectifying effect and reduction of the apparent critical current density can be explained. From the viewpoint of the flux motion, since the electric field, $\boldsymbol{E} = \boldsymbol{B} \times \boldsymbol{v}$,

is along the y-axis and the magnetic flux density $\boldsymbol{B}$ is almost parallel to the x-axis, the velocity of flux lines is approximately directed along the negative z-axis. That is, the flux lines flow in the negative z-axis direction with an oscillating motion in the x-z plane. The details of this flux motion are described in [16]. In this reference the more general theoretical analysis of the force balance equation including the viscous force was carried out and an approximate solution expressed in a power series in frequency was obtained as in the last section. The obtained current-voltage characteristics were compared with experimental results.

3.3.2 Reversible Magnetization

Even for a superconductor with a hysteretic magnetization due to flux pinning, it is known [18] that the superposition of small parallel AC and DC magnetic fields results in a reduction of the hysteresis of the DC magnetization or sometimes even in reversible magnetization (see Fig. 3.13). Figure 3.14(a) shows the variation of the magnetic flux distribution in a superconductor during one cycle of the AC field in the presence of an increasing DC field. For simplicity the diamagnetism is disregarded and the Bean-London model is assumed for the pinning force density. The magnetic flux distribution averaged over one cycle is shown in Fig. 3.14(b); it is flatter than that in the absence of the AC field itself (represented by the broken line). Thus, the reduction in magnetization hysteresis can be explained. The magnitude of the hysteresis is predicted to be

$$\Delta M = \Delta M_0 \left(1 - \frac{h_0}{H_\mathrm{p}}\right)^2, \tag{3.42}$$

where ΔM_0 is the hysteretic magnetization in the absence of the AC field. Hence, when the AC field amplitude h_0 exceeds the penetration field H_p, the hysteresis disappears and the magnetization becomes reversible. This method is useful for investigation of the diamagnetism in superconductors.

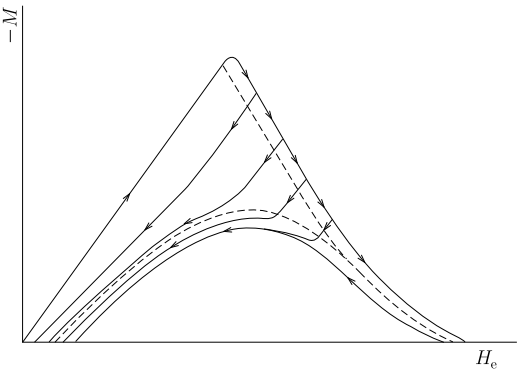

Fig. 3.13 Magnetization of a superconducting Pb-1.92at%Tl cylinder [18]. *Broken* and *solid lines* correspond to the cases with and without the superposition of small AC magnetic field, respectively

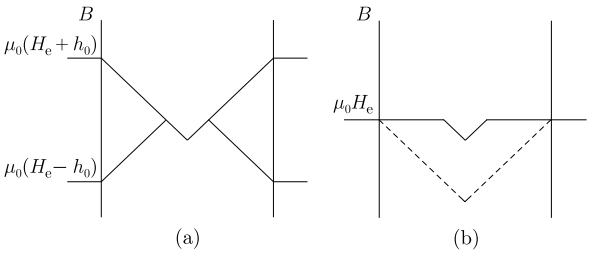

Fig. 3.14 (**a**) Maximum flux density (*upper line*) and minimum one (*lower line*) during one period of AC magnetic field of amplitude h_0 in an increasing DC magnetic field H_e. (**b**) The *solid line* shows averaged magnetic flux density in one period and the *broken line* corresponds to the case without the AC magnetic field

3.3.3 Abnormal Transverse Magnetic Field Effect

When the AC magnetic field is superposed normal to the transverse DC field applied to a superconducting cylinder or tape as shown in Fig. 3.15, the magnetization due to the transverse DC field decreases gradually. Such a phenomenon is called the "abnormal transverse magnetic field effect" [19–21]. An example is shown in Fig. 3.16 where the AC field is applied parallel to a superconducting cylinder: (a) and (c) correspond to the processes of increasing and decreasing DC field, respectively. (b) depicts field cooled process wherein the DC field is applied at a temperature higher than the critical value T_c, and then the temperature is decreased below T_c. The initial magnetic flux distribution due to the application of the DC field in each case is shown in the right side of the figure. The magnetization decreases with application of the AC field and reduces approximately to zero in the steady state.

When the AC field is superposed in a different direction from the DC field as above-mentioned, it is necessary to obtain the distribution of the shielding current. If we assume that the current flows so as to shield the penetration of AC field as much as possible, the current that has shielded the DC field now has to change completely to shield the AC field, resulting in a complete penetration of the DC field. In this

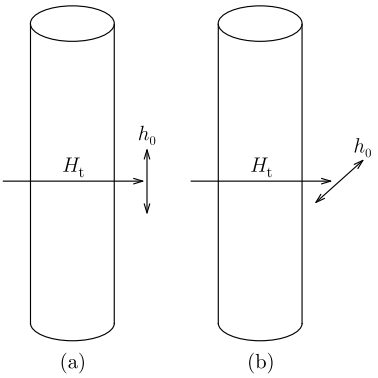

Fig. 3.15 Application of transverse magnetic field H_t and normal small AC magnetic field h_0 to a superconducting cylinder

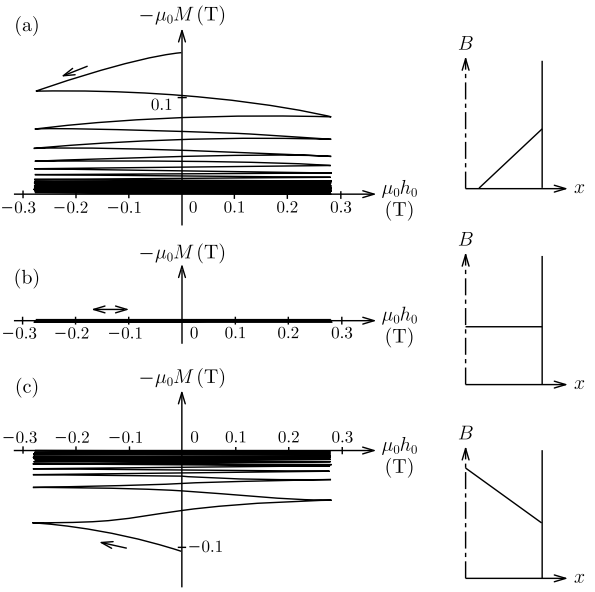

Fig. 3.16 Relaxation of longitudinal magnetization [19] due to superposition of AC magnetic field shown in Fig. 3.15(a) in the processes of (**a**) increasing field, (**b**) field cooling and (**c**) decreasing field. *Right figures* show the initial distributions of DC magnetic flux in each process

case the total amount of penetrating flux seems to be very large. Hence, the shielding current is predicted to flow in such a way that the total amount of penetrating DC and AC flux is minimum. Then, a part of the current that has shielded only the DC field changes so as to shield the AC field. In other words, a flowing pattern of the current changes gradually from one that shields the DC field to one that shields the AC field during each successive half-cycle of the AC field. Figure 3.17 represents the varying states of distribution of the shielding current when the AC field is applied normal to the superconducting cylinder. Therefore, the DC field penetrates gradually one cycle after another until complete penetration is finally reached. In this final state

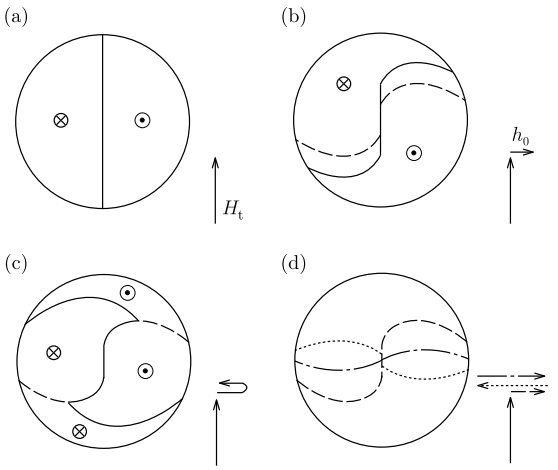

Fig. 3.17 Variation of the distribution of shielding current in the order from (**a**) to (**d**) due to the superposition of AC magnetic field shown in Fig. 3.15(b)

the current shields only the AC field. The abnormal transverse magnetic field effect is a kind of relaxation process in which the direction of the magnetic moment due to the shielding current changes gradually. In the field cooled process shown in Fig. 3.16(b) the DC field has already penetrated hence the current flows so as to fully shield the AC field.

3.4 Flux Jump

The magnetization in a superconductor sometimes varies discontinuously during the sweeping of a magnetic field as shown in Fig. 3.18. This phenomenon is called the flux jump. An example of the observed magnetic flux distribution inside a flux-jumping superconductor [22] is shown in Fig. 3.19. It is seen from this observation that the disappearance of shielding current in the superconductor at the moment of the flux jump is accompanied by a sudden invasion of the magnetic flux. Such an instability originates from the irreversible nature of flux pinning. For instance, we assume that a local flux motion occurs for some reason. This will lead to some energy dissipation and a slight temperature rise. This temperature rise will reduce the pinning force that prevents the flux motion and more flux lines than the initial group will move. This will cause a further energy dissipation and temperature rise. The phenomenon will continue until such positive feedback destroys the superconductivity and the flux motion is completely stopped. This is an outline of the mechanism of flux jumping.

In metallic superconductors the diffusion velocity of the heat is usually much faster than that of the flux lines. Hence, the isothermal approximation is adequate for a superconductor. Thus we assume that the temperature T is uniform throughout the superconductor. The heat produced in the superconductor by the flux motion is absorbed into a coolant such as liquid helium; the equation of heat flow is

$$P = C\frac{\mathrm{d}T}{\mathrm{d}t} + \Phi_{\mathrm{h}}, \tag{3.43}$$

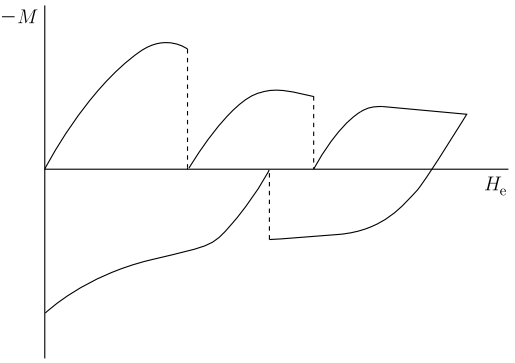

Fig. 3.18 Discontinuous variation of the magnetization due to flux jumping

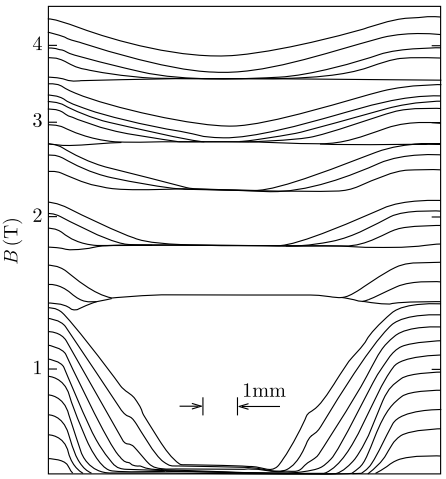

Fig. 3.19 Variation of the magnetic flux distribution in a Nb-Ti measured by scanning a Hall probe in a gap between two pieces of specimen [22]

where P is the power loss density in the superconductor, C is the heat capacity of a unit volume of the superconductor and Φ_h is the heat flux absorbed by the coolant. When the temperature of the superconductor is not much higher than the temperature of the coolant T_0, the heat flux to the coolant is given by $\Phi_\mathrm{h} = K(T - T_0)$, where K is the heat transfer coefficient per unit volume of the superconductor. Viscous loss and related quantities are disregarded. P contains not only the pinning power loss density P_0 at constant temperature but also an additional component, $C_\mathrm{p}(\mathrm{d}T/\mathrm{d}t)$, due to the temperature rise. The temperature rise causes a variation in the parameter α_c, the flux pinning strength. The resultant variation in the magnetic flux distribution is obtained from (2.47) as

$$\delta \widehat{B}^{1-\gamma} \frac{\partial \widehat{B}}{\partial T} = -\mu_0 \frac{\mathrm{d}\alpha_\mathrm{c}}{\mathrm{d}T} x. \tag{3.44}$$

From (2.75) the additional power loss density is

$$P_1 = -\alpha_\mathrm{c} \widehat{B}^{\gamma-1} \frac{\mathrm{d}T}{\mathrm{d}t} \int_{x_\mathrm{b}}^{x} \delta \frac{\partial \widehat{B}}{\partial T} \mathrm{d}x. \tag{3.45}$$

Equations (2.47) and (3.44) are substituted into (3.45) and after some calculation we obtain the mean power loss density:

$$\langle P_1 \rangle = \frac{1}{d} \int_0^{x_\mathrm{b}} P_1 \mathrm{d}x \equiv C_\mathrm{p} \frac{\mathrm{d}T}{\mathrm{d}t}. \tag{3.46}$$

Here we assume the Bean-London model ($\gamma = 1$). In case the magnetic flux penetrates to the center of a superconducting slab of thickness $2d$ as in Fig. 3.20, we have $\delta_0 = \delta_\mathrm{b} = 1$ in the region $0 \le x \le d$ and $x_\mathrm{b} = d$, and C_p is given by

$$C_\mathrm{p} = \frac{1}{3} \mu_0 H_\mathrm{p} \left(-\frac{\mathrm{d}H_\mathrm{p}}{\mathrm{d}T} \right). \tag{3.47}$$

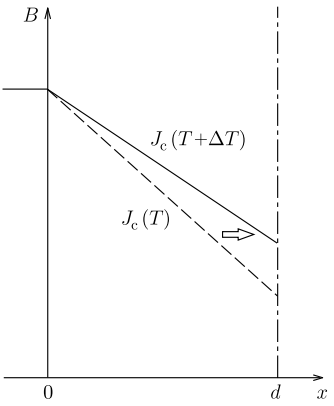

Fig. 3.20 Variation of the magnetic flux distribution in a superconducting slab when the temperature is changed by ΔT

Because of this term (3.43) is rewritten as

$$(C - C_p)\frac{dT}{dt} = P_0 - \Phi_h. \tag{3.48}$$

According to this equation the rate of temperature rise, dT/dt, diverges when

$$C - C_p = 0 \tag{3.49}$$

is satisfied. This is the condition of the rapid temperature rise, i.e., the flux jump.

Yamafuji et al. [23] discussed the temperature rise in detail, taking account a higher order term $(dT/dt)^2$ which originated from the viscous loss. According to their argument the condition that dT/dt becomes indefinite must be satisfied for a flux jump to occur. This means that the condition

$$P_0 - \Phi_h = 0 \tag{3.50}$$

must be satisfied simultaneously with the heat-capacity condition of (3.49). However, the validity of (3.50) has not yet been clarified. Anyhow (3.49) is the condition for the flux jump.

Since flux jumping reduces the critical current density to zero, it must be avoided in practical superconducting wires. Hence, the inequality that $C > C_p$ is required so that (3.49) cannot be satisfied. Since $H_p = J_c d$, this inequality is equivalent to

$$d < \left[\frac{\mu_0}{3C}\left(-\frac{dJ_c}{dT}\right)J_c\right]^{-1/2} \equiv d_c. \tag{3.51}$$

This implies that the thickness of superconductor $2d$ should be less than $2d_c$. This is the principle of stabilization of superconducting wire by reduction of the superconducting filament diameter. In practical superconducting wires, many fine superconducting filaments are embedded in matrix materials such as copper and are stabilized by the above principle. At the same time the high thermal conductivity of the matrix

material ensures rapid dissipation of generated heat. In the case of Nb_3Sn for example, if we assume that $J_c = 1 \times 10^{10}\ \mathrm{A\,m^{-2}}$, $-\mathrm{d}J_c/\mathrm{d}T = 7 \times 10^8\ \mathrm{A\,m^{-2}\,K^{-1}}$ and $C = 6 \times 10^3\ \mathrm{J\,m^{-3}\,K^{-1}}$, we have $2d < 90\ \mu\mathrm{m}$ from (3.51). In practical multifilamentary Nb_3Sn wires the diameter of superconducting filaments is smaller than several 10 μm. The filament diameter in multifilamentary wires for AC use is sometimes reduced below 1 μm to reduce the hysteresis loss drastically.

The condition of stabilization (3.51) can also be derived from the following simple argument. Again consider the magnetic flux distribution shown in Fig. 3.20 and assume that the temperature in the superconductor rises from T to $T + \Delta T$ within a short period of time, Δt. The resultant change in critical current density is then $\Delta J_c = (\mathrm{d}J_c/\mathrm{d}T)\Delta T$, where of course $\Delta J_c < 0$. Hence, the magnetic flux distribution changes as shown in Fig. 3.20 and the induced electric field due to this change is

$$E(x) = \int_d^x \mu_0 \frac{\Delta J_c}{\Delta t} x \mathrm{d}x = \frac{\mu_0}{2}\left(-\frac{\Delta J_c}{\Delta t}\right)\left(d^2 - x^2\right). \tag{3.52}$$

The resultant energy loss density is given by

$$W = \frac{1}{d}\int_0^{\Delta t} \mathrm{d}t \int_0^d J_c E(x)\mathrm{d}x = \frac{\mu_0}{3}\left(-\frac{\mathrm{d}J_c}{\mathrm{d}T}\right) J_c d^2 \Delta T. \tag{3.53}$$

If Δt is sufficiently small, the above variation is supposed to occur adiabatically. In this case the additional temperature rise in the superconductor is estimated to be $\Delta T' = W/C$. Provided that this temperature rise $\Delta T'$ is smaller than the initial temperature rise ΔT, the initial disturbance will not develop into a flux jump by positive feedback. This condition agrees with (3.51).

3.5 Surface Irreversibility

During measurement of the DC magnetization of a superconductor, when the sweep of the external magnetic field changes from increasing to decreasing, the magnetization curve is sometimes linear with slope -1 over a certain range of field variation denoted by ΔH, as shown in Fig. 3.21. This is similar to the variation of magnetization in the Meissner state. That is, the magnetic flux distribution is macroscopically unchanged during the variation of the external field. If the external field is increased again within this range, the magnetization reverses. It should be noted, however, that, although in the usual magnetization measurement the magnetization seems to behave reversible as in Fig. 3.21, sensitive B-H_e measurements in fact reveal it to be irreversible. Such behavior is also observed when the sweep of external field changes from decreasing to increasing. This phenomenon insists that an irreversible current with a very high density flows in the surface region and shields the variation of the external field. The magnitude of the magnetization ΔH due to the surface current is sample dependent and varies with the magnetic field; ΔH usually decreases with increasing field.

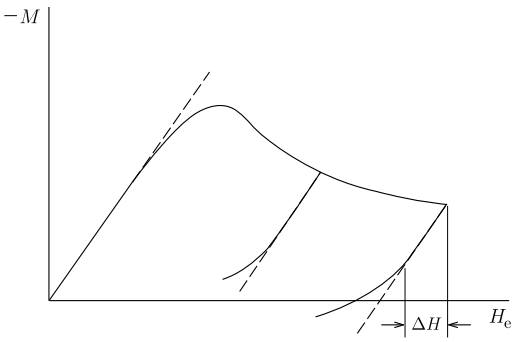

Fig. 3.21 Macroscopic magnetization due to the surface irreversibility

Three mechanisms, viz. surface sheath, surface barrier, and surface pinning have been proposed to explain the irreversible surface current.

The surface superconductivity treated in Sect. 1.6 is associated with a special property of the surface which permits the superconducting order parameter to take on a nonzero value even when the applied magnetic field is above H_{c2}. Fink [24] speculated that a similar two-dimensional surface superconductivity exists even below H_{c2} independently of the three-dimensional flux line structure inside the superconductor. This surface superconductivity is called the surface sheath and considered to cause an irreversible surface current.

The idea of a "surface barrier" was proposed by Bean and Livingston [25] who suggested that the surface itself provided a barrier against the invasion and elimination of flux lines. The surface barrier was originally proposed during investigations of the first entry field of flux lines into a practical superconductor in comparison with H_{c1}, the theoretical result of Abrikosov for an infinitely large superconductor. We begin by assuming that a flux line has entered the superconductor from the surface. In addition to the external field that decays within a characteristic distance of λ from the surface we consider the flux line, and a postulated image flux line directed opposite to it as in Fig. 3.22. The image is necessary to fulfill the boundary condition that the current around the flux line should not flow across to the surface. The total magnetic flux of the flux line (the component of b in Fig. 3.22) is smaller than the flux quantum ϕ_0 and hence, flux quantization is not fulfilled. This is because the current is not zero on the surface, which is a part of the loop enclosing the magnetic flux.

Bean and Livingston treated the case where the G-L parameter κ is large, in which case the modified London equation is valid and the magnetic flux density of the flux line penetrating sufficiently deeply from the surface is given by (1.61). We assume that the superconductor occupies $x \geq 0$ and the external magnetic field H_e is applied parallel to the z-axis. The position of the flux line in the x-y plane is represented as $(x_0, 0)$, where $x_0 > 0$. Its image is located at $(-x_0, 0)$ and the total magnetic flux density in the superconductor is given by

$$b = \mu_0 H_e \exp\left(-\frac{x}{\lambda}\right) + \frac{\phi_0}{2\pi\lambda^2}\left[K_0\left(\frac{\sqrt{(x-x_0)^2+y^2}}{\lambda}\right)\right.$$

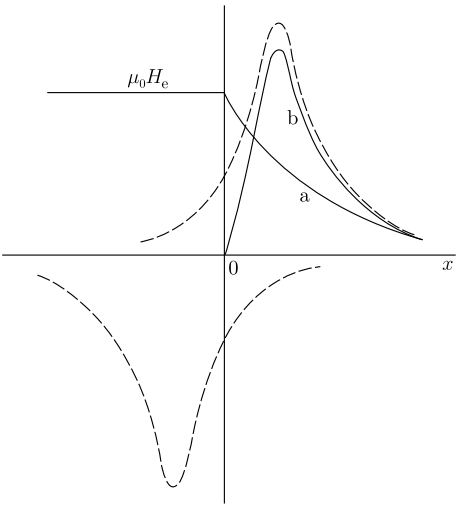

Fig. 3.22 Surface barrier model by Bean and Livingston [25]. 'a' represents the penetrating magnetic flux from the surface given by (1.14) and 'b' is the sum of the penetrating flux line and its image

$$- K_0\left(\frac{\sqrt{(x+x_0)^2+y^2}}{\lambda}\right)\Bigg] \tag{3.54}$$

except the region of the normal core. The Gibbs free energy is given by

$$G = \int \left\{ \frac{1}{2\mu_0}\left[\boldsymbol{b}^2 + \lambda^2(\nabla \times \boldsymbol{b})^2\right] - \boldsymbol{H}_e \cdot \boldsymbol{b} \right\} \mathrm{d}V, \tag{3.55}$$

where the volume integral is over the superconductor ($x \geq 0$). The first term in (3.54) may be symbolized by $\boldsymbol{b}_0$ and the sum of the second and third terms which represent the penetrating flux line and its image may be symbolized by $\boldsymbol{b}_1$. After substituting these into (3.55), partially integrating and using the modified London equation, the Gibbs free energy becomes

$$\begin{aligned} G = {} & \lambda^2 \int_S (\nabla \times \boldsymbol{b}_1) \times \boldsymbol{H}_e \cdot \mathrm{d}\boldsymbol{S} \\ & + \frac{\lambda^2}{2\mu_0} \int_{S_c} \left[\boldsymbol{b}_1 \times (\nabla \times \boldsymbol{b}_1) + 2\boldsymbol{b}_1 \times (\nabla \times \boldsymbol{b}_0) + 2\mu_0 (\nabla \times \boldsymbol{b}_1) \times \boldsymbol{H}_e\right] \cdot \mathrm{d}\boldsymbol{S} \\ & + \frac{1}{2\mu_0} \int_{\Delta V} \left[\boldsymbol{b}_1^2 + \lambda^2 (\nabla \times \boldsymbol{b}_1)^2 + 2\boldsymbol{b}_0 \cdot \boldsymbol{b}_1 + 2\lambda^2 (\nabla \times \boldsymbol{b}_0) \cdot (\nabla \times \boldsymbol{b}_1) \right. \\ & \left. - 2\mu_0 \boldsymbol{b}_1 \cdot \boldsymbol{H}_e\right] \mathrm{d}V. \end{aligned} \tag{3.56}$$

In the above the first integral is carried out on the surface of superconductor, S($x = 0$), the second one on the surface of normal core of the flux line, S_c ($\mathrm{d}\boldsymbol{S}$ is directed inward the surface), and the third one inside the normal core. The constant terms which are functions only of $\boldsymbol{b}_0$ are omitted. In the first integral in (3.56), since $\boldsymbol{H}_e$ is equal to $\boldsymbol{b}_0/\mu_0$ on the surface, it can be replaced by $\boldsymbol{b}_0/\mu_0$. If we replace the

integral on S to an integral on S and S_c minus an integral on S_c, we have

$$\frac{\lambda^2}{\mu_0}\int_{S+S_c}(\nabla\times\boldsymbol{b}_1)\times\boldsymbol{b}_0\cdot\mathrm{d}\boldsymbol{S}=\frac{\lambda^2}{\mu_0}\int_{S+S_c}(\nabla\times\boldsymbol{b}_0)\times\boldsymbol{b}_1\cdot\mathrm{d}\boldsymbol{S}$$
$$-\frac{\lambda^2}{\mu_0}\int_{S_c}(\nabla\times\boldsymbol{b}_0)\times\boldsymbol{b}_1\cdot\mathrm{d}\boldsymbol{S}, \tag{3.57}$$

where partial integration is done and the modified London equation and the boundary condition of $\boldsymbol{b}_1=0$ on the superconductor surface are used. Thus, (3.56) reduces to

$$G=\frac{\lambda^2}{2\mu_0}\int_{S_c}\left[\boldsymbol{b}_1\times(\nabla\times\boldsymbol{b}_1)-2\mu_0\boldsymbol{H}_e\times(\nabla\times\boldsymbol{b}_1)+2\boldsymbol{b}_0\times(\nabla\times\boldsymbol{b}_1)\right]\cdot\mathrm{d}\boldsymbol{S}$$
$$+\frac{1}{2\mu_0}\int_{\Delta v}\left[\boldsymbol{b}_1^2+\lambda^2(\nabla\times\boldsymbol{b}_1)^2+2\boldsymbol{b}_0\cdot\boldsymbol{b}_1+2\lambda^2(\nabla\times\boldsymbol{b}_0)\cdot(\nabla\times\boldsymbol{b}_1)\right.$$
$$\left.-2\mu_0\boldsymbol{b}_1\cdot\boldsymbol{H}_e\right]\mathrm{d}V. \tag{3.58}$$

Now we write $\boldsymbol{b}_1=\boldsymbol{b}_f+\boldsymbol{b}_i$ to indicate the sum of the flux line and its image, where the full expressions for these components are just the second and third terms in (3.54). After a simple calculation we have

$$G=\frac{\lambda^2}{2\mu_0}\int_{S_c}\left[\boldsymbol{b}_f\times(\nabla\times\boldsymbol{b}_f)+\boldsymbol{b}_i\times(\nabla\times\boldsymbol{b}_f)-\boldsymbol{b}_f\times(\nabla\times\boldsymbol{b}_i)\right.$$
$$\left.-2\mu_0\boldsymbol{H}_e\times(\nabla\times\boldsymbol{b}_f)+2\boldsymbol{b}_0\times(\nabla\times\boldsymbol{b}_f)-2\boldsymbol{b}_f\times(\nabla\times\boldsymbol{b}_0)\right]\cdot\mathrm{d}\boldsymbol{S}$$
$$+\frac{1}{2\mu_0}\int_{\Delta v}\left[\boldsymbol{b}_f^2+\lambda^2(\nabla\times\boldsymbol{b}_f)^2-2\mu_0\boldsymbol{b}_f\cdot\boldsymbol{H}_e\right]\mathrm{d}V. \tag{3.59}$$

With the aid of (1.78) it turns out that the sum of the first term in the first integral and the first and second terms in the second integral gives the self energy of the flux line, $\epsilon=\phi_0 H_{c1}$, and the sum of the fourth term in the first integral and the third term in the second integral gives a constant term, $-\phi_0 H_e$. The fifth and second terms in the first integral represent the interactions of the flux line with the Lorentz force due to the surface current and with the image, respectively. It can be easily shown that the third and sixth terms in the first integral are sufficiently small and can be disregarded. Thus, we have

$$G=\phi_0\left[H_e\exp\left(-\frac{x_0}{\lambda}\right)-\frac{\phi_0}{4\pi\mu_0\lambda^2}K_0\left(\frac{2x_0}{\lambda}\right)+H_{c1}-H_e\right] \tag{3.60}$$

(per unit length of the flux line), which is identical with the result obtained by Bean and Livingston [25] and by de Gennes [26]. This equation is valid for the case where the normal core completely penetrates the superconductor, i.e., $x_0>\xi$. Since the constant term that depends only on $\boldsymbol{b}_0$ is omitted, we have $G=0$ when the flux line

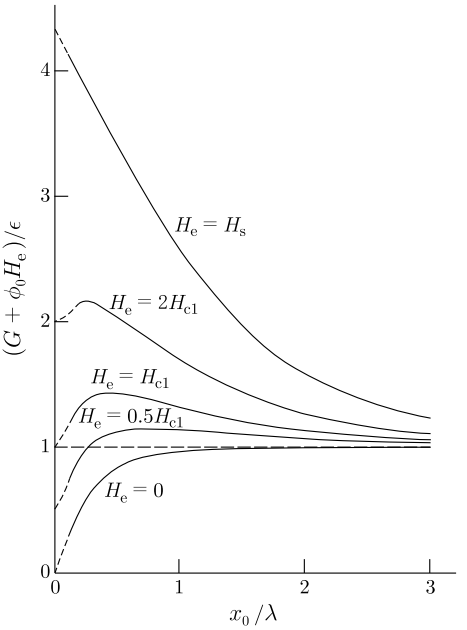

Fig. 3.23 Variation of the energy G vs. the position, x_0, of the flux line in case $\kappa = 10$ [25]. The ordinate is normalized by the self energy, ϵ, of flux line per unit length

does not penetrate the superconductor, i.e., $x_0 = 0$. When $H_e = H_{c1}$, G goes to zero in the limit $x_0 \to \infty$. That is, the condition of a bulk superconductor is naturally satisfied.

Figure 3.23 shows the variation in the free energy G with the position of the flux line x_0. It means that the energy barrier exists even when H_e exceeds H_{c1} and the flux line cannot penetrate the superconductor. Hence, the magnetization remains perfectly diamagnetic until the external magnetic field reaches H_s sufficiently greater than H_{c1}, and then the flux line first penetrates. Conversely, the surface barrier prevents the flux lines from exiting the superconductor as the field decreases. The flux lines are predicted to be trapped in the superconductor until the external field is reduced to zero. Also in this case the magnetization curve is a line parallel to the Meissner line, suggesting that the internal magnetic flux distribution remains unchanged even under variation of the external field. Such feature agrees qualitatively with the surface irreversibility phenomenon observed experimentally. For this reason the surface barrier model seems to be applicable not only to the estimation of the first penetration field, its initial purpose, but also to the general phenomena of surface irreversibility.

Here, we shall estimate the first penetration field H_s of the flux line from the above result of the Bean-Livingston model. We treat the case in which the flux line exists near the surface ($x_0 \sim \xi$). The corresponding magnetic flux density is approximately given by (1.62a). Thus, the Gibbs free energy reduces to

$$G = \phi_0 \left[H_e \exp\left(-\frac{x_0}{\lambda}\right) + \frac{\phi_0}{4\pi\mu_0\lambda^2} \log 2x_0 \right] + \text{const.} \tag{3.61}$$

Since the penetration of flux line occurs when $\partial G/\partial x_0 = 0$ is attained at $x_0 \sim \xi$, we have

$$H_s \simeq \frac{\phi_0}{4\pi\mu_0\lambda\xi} = \frac{H_c}{\sqrt{2}}. \tag{3.62}$$

The calculation in terms of the modified London equation in the above is not exact when x_0 is close to ξ. Then, de Gennes [27] argued the first penetration field H_s using the G-L equations. We assume again that the superconductor occupies $x \geq 0$. de Gennes treated this problem as an extrapolation of the Meissner state above H_{c1}, i.e., the superheated state and assumed that the order parameter and the vector potential vary one-dimensionally only along the x-axis. In this case, the order parameter can be chosen as a real number as known well. If we normalize Ψ by $|\Psi_\infty|$ as in (1.38) and the vector potential $\boldsymbol{A}$ and the coordinate x as

$$\boldsymbol{a} = \frac{\boldsymbol{A}}{\sqrt{2}\mu_0 H_c \lambda}, \tag{3.63}$$

$$\tilde{x} = \frac{x}{\lambda}, \tag{3.64}$$

the G-L equations (1.30) and (1.31) reduce to

$$\frac{1}{\kappa^2}\cdot\frac{\mathrm{d}^2\psi}{\mathrm{d}\tilde{x}^2} = \psi\left(-1+\psi^2+a^2\right), \tag{3.65}$$

$$\frac{\mathrm{d}^2 a}{\mathrm{d}\tilde{x}^2} = \psi^2 a. \tag{3.66}$$

In the above, a is the y-component of $\boldsymbol{a}$, if the magnetic field is applied along the z-axis. As will be shown later, ψ and a vary gradually with the distance of the order of 1 in the $\tilde{x}$-coordinate (λ in real space). Hence, the left-hand side of (3.65) can be approximately replaced by zero for a superconductor with the large G-L parameter κ. Then, (3.65) reduces to

$$\psi^2 = 1 - a^2. \tag{3.67}$$

Substitution of this into (3.66) leads to

$$\frac{\mathrm{d}^2 a}{\mathrm{d}\tilde{x}^2} = a - a^3. \tag{3.68}$$

Multiplying both sides by $\mathrm{d}a/\mathrm{d}\tilde{x}$ and integrating, we have

$$\left(\frac{\mathrm{d}a}{\mathrm{d}\tilde{x}}\right)^2 - a^2 + \frac{a^4}{2} = \text{const.} \tag{3.69}$$

Since a and $\mathrm{d}a/\mathrm{d}\tilde{x}$ are expected to drop to zero at deep inside the superconductor, $\tilde{x} \to \infty$, the constant term on the right-hand side of (3.69) must be zero. Thus,

$$a = -\frac{\sqrt{2}}{\cosh(\tilde{x} + c)}, \tag{3.70}$$

where c is a constant determined by the boundary condition at the surface, $\tilde{x} = 0$. This solution satisfies the above-mentioned requirement that the physical quantities vary gradually with the distance of the order of λ in real space. From (3.70) the magnetic flux density is

$$B = \sqrt{2}\mu_0 H_\mathrm{c} \frac{\mathrm{d}a}{\mathrm{d}\tilde{x}} = \frac{2\mu_0 H_\mathrm{c} \sinh(\tilde{x} + c)}{\cosh^2(\tilde{x} + c)}. \tag{3.71}$$

From the boundary condition that the magnetic flux density is $\mu_0 H_\mathrm{e}$ at $\tilde{x} = 0$, c can be evaluated from

$$\frac{H_\mathrm{c}}{H_\mathrm{e}} = \frac{2 \sinh c}{\cosh^2 c}. \tag{3.72}$$

The maximum value of H_e, i.e., the first penetration field, H_s, corresponds to $c = \sinh^{-1} 1$, and hence [27]

$$H_\mathrm{s} = H_\mathrm{c}. \tag{3.73}$$

If we neglect the term proportional to $(\mathrm{d}\psi/\mathrm{d}\tilde{x})^2$, the free energy density is given by

$$\begin{aligned} F &= \mu_0 H_\mathrm{c}^2 \left[-\psi^2 + \frac{1}{2}\psi^4 + \left(\frac{\mathrm{d}a}{\mathrm{d}\tilde{x}} \right)^2 + a^2 \psi^2 \right] \\ &= \mu_0 H_\mathrm{c}^2 \left[-\frac{1}{2} + \frac{4 \sinh^2(\tilde{x} + c)}{\cosh^4(\tilde{x} + c)} \right] \end{aligned} \tag{3.74}$$

or

$$F = -\frac{1}{2}\mu_0 H_\mathrm{c}^2 + \frac{B^2}{\mu_0} = F_\mathrm{n} - \frac{1}{2}\mu_0 H_\mathrm{c}^2 + \frac{B^2}{2\mu_0}, \tag{3.75}$$

where $F_\mathrm{n} = B^2/2\mu_0$ is the energy density of magnetic field, i.e., the free energy density in the normal state. Figure 3.24 shows the magnetic flux density, the normalized order parameter and the free energy density in the critical state at $H_\mathrm{e} = H_\mathrm{c}$. At the surface where the magnetic flux density reaches $\mu_0 H_\mathrm{c}$, the order parameter ψ is zero and the free energy density F is equal to F_n, its normal-state value.

As shown above the first penetration fields, as obtained by Bean and Livingston and by de Gennes, are of the order of H_c, although these differ by a factor of $\sqrt{2}$. In the case of high-κ superconductors, which is the required condition for the approximations, the predicted values are much greater than the bulk value, $H_{\mathrm{c}1}$. Such large penetration fields have not yet been observed.

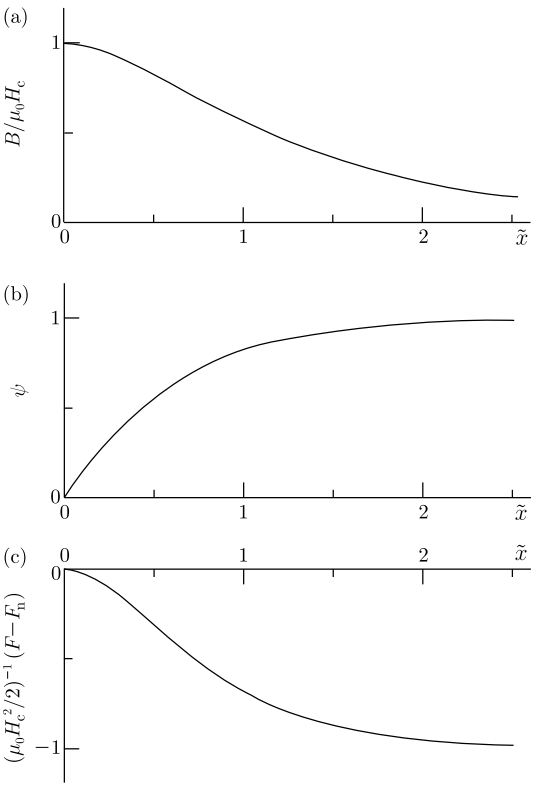

Fig. 3.24 (**a**) Magnetic flux density, (**b**) normalized order parameter and (**c**) free energy density in the vicinity of the surface of a superconductor in the critical superheated state ($H_e = H_c$)

Here the relationship between the two theories will be discussed. As mentioned above the superheated state has been treated by de Gennes. In this case, the assumption that the order parameter gradually varies one-dimensionally does not hold any more as the field decreases after the penetration of flux lines, and hence, the superheated state cannot be re-established. It follows that the magnetization curve is predicted to be reversible after the penetration of flux lines, as shown in Fig. 3.25. Hence, in oder to discuss the surface irreversibility, the interaction between the flux line and the surface should be treated as it was done in the surface barrier model. It is also important to investigate the effect of surface roughness. If the surface roughness is of the order of ξ, it is accompanied by a steep spatial variation of Ψ, in which case the assumption of a gradual one-dimensional variation is no longer valid. In high κ superconductors, ξ is small and it seems to be quite difficult to make the surface roughness of bulk specimens smaller than ξ. Hence, it seems unphysical to image that the superheated state could be maintained up to high fields. On the other hand, the penetration of flux line results in a two-dimensional spatial variation of Ψ and the surface barrier appears. In this case the image of flux line is considered to become dim due to the surface roughness resulting in a weakening of the interaction between the flux line and its image. However, the surface barrier should remain. Thus, it can be seen that there is a difference between the surface barrier mechanism

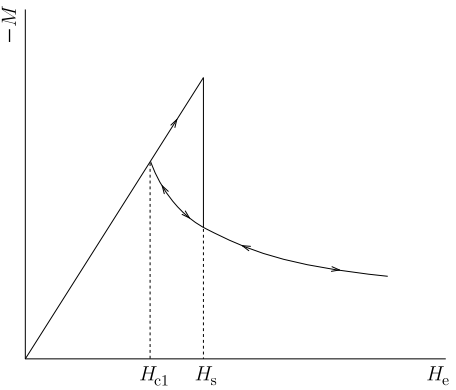

Fig. 3.25 Magnetization after the superheated state is destroyed

and the superheating mechanisms proposed by de Gennes, and furthermore that the former provides a more practical explanation of surface irreversibility.

When the surface is roughened, it is speculated that the effects of surface sheath and surface barrier are reduced. However, the surface irreversibility is enhanced in most cases. It has been shown that neither bulk irreversibility nor surface irreversibility is observed in materials with few defects and clean surfaces [28], indicating that the surface sheath and the surface barrier are not the main causes of surface irreversibility. On the other hand, Hart and Swartz [29] speculated that the pinning by surface roughness and defects near the surface causes the surface irreversibility based on the correlation between the surface roughness and the irreversibility. This mechanism is called "surface pinning."

Experimentally it has been shown that surface pinning is a dominant mechanism. Matsushita et al. [30][1] showed that residual pinning centers could be removed from several Nb-50at%Ta tape specimens by heat treatment at very high temperatures under very high vacuum. After this heat treatment, dislocations with different densities were introduced to the specimens by different rates of rolling deformation. The initial thickness of each specimen was changed so that the final thicknesses of all the specimens were the same. Since the superconducting properties such as T_c and H_c and the condition of the surface were almost the same in each one, ΔH should have been approximately the same, if either the surface sheath or the surface barrier was the origin of the surface irreversibility. Figure 3.26 shows the bulk critical current density J_c and the one near the surface J_{cs} estimated using Campbell's method described in Sect. 5.3, where J_{cs} is approximately proportional to ΔH. This result shows that not only the bulk critical current density, J_c, but also the surface one J_{cs} increases significantly with increasing density of pinning dislocations and that the two critical current densities are saturated to almost the same value in the strong pinning limit. From the fact that the surface irreversibility is enhanced by two orders of magnitude by introduction of dislocations, it can be concluded that the dominant cause of the surface irreversibility is surface pinning and that the effects of a

[1] As to the magnetic field dependence of surface critical current density, see [31].

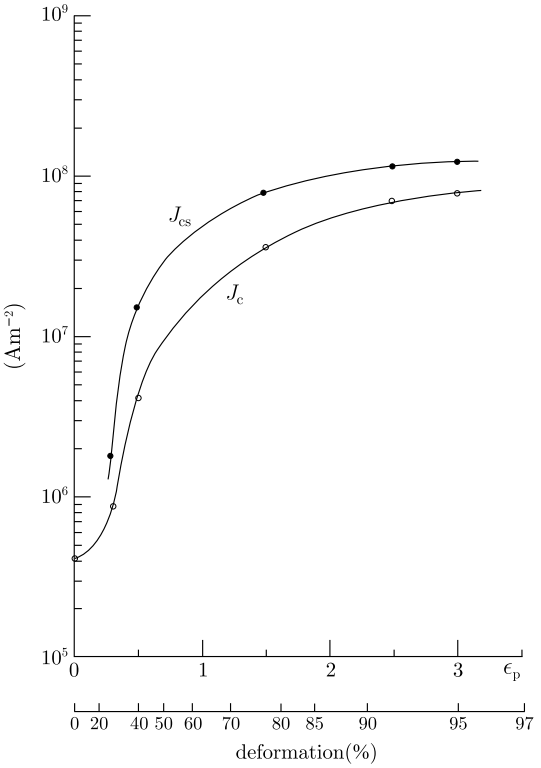

Fig. 3.26 Bulk critical current density J_c and surface one J_{cs} vs. deformation by the cold rolling in Nb-Ta specimens [30]. These critical current densities increase with increasing density of pinning dislocations. The deformation is defined as $1-(A_0/A)$ and we have $\epsilon_p = \log(A/A_0)$, where A and A_0 represent the surface area of superconductor before and after the rolling, respectively

surface barrier etc. can be neglected. In addition, a saturation behavior of critical current density in the strong pinning regime and its special magnetic field dependence [30, 31] are known to be characteristic features of the saturation phenomenon for the bulk flux pinning, which will be described in Sect. 7.5.

It has been concluded that since with rolling deformation the defects are nucleated with the higher density in the surface region, the surface critical current density J_{cs} increases faster than the bulk value.

It follows that the surface irreversibility is not an intrinsic surface effect as such but rather a secondary phenomenon caused by defects that are likely to be concentrated in the surface region. It is generally known [30, 31] that the magnitude of surface irreversibility ΔH decreases with increasing magnetic field and disappears at high fields. This is caused by the nonlocal nature of the flux pinning. That is, the critical current density is a value averaged over the range of the pinning correlation length of the flux line lattice (Campbell's AC penetration depth that will be described in the next section). At high fields, this correlation length increases, and the region of the average is no longer limited to the surface region with strong pinning forces but extends into the inner region. Thus, the surface irreversibility is diluted quickly with increasing magnetic field strength.

As discussed above, surface pinning rather than the surface barrier effect is the dominant mechanism of surface irreversibility. As indicated in Fig. 3.23 the energy

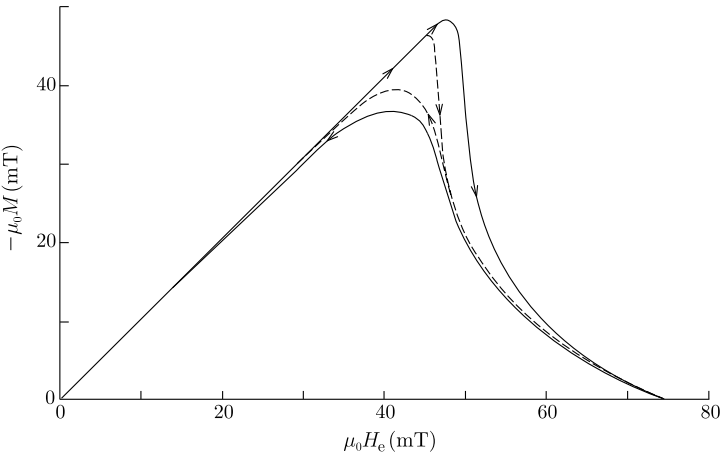

Fig. 3.27 Magnetization of V specimen at 4.2 K [33]. *Solid* and *broken lines* show results on the specimen before and after the oxygenation, respectively

barrier itself is not particularly large, and in any case its effectiveness reduces in the presence of the usual surface roughness which by dimming the image of flux line weakens the attraction between the flux line and the image. In addition, the penetration of flux lines through the surface barrier can be facilitated by flux creep, to be discussed in Sect. 3.8.

The surface pinning force itself can be reduced by various kinds of surface treatments such as metallic coating [32] or oxidation [33] (see Fig. 3.27). In the former case, a proximity effect between the normal metal coating and the superconductor reduces the order parameter at the surface and hence the strength of surface pinning.

3.6 DC Susceptibility

Measurement of DC susceptibility in the field cooled process was carried out for evaluating the superconducting volume fraction of a specimen just after the discovery of high-temperature superconductors. A constant susceptibility at sufficiently low temperatures was regarded as related to the volume fraction of a superconducting phase. However, this is correct only for pin-free superconductors. As the temperature decreases, the superconductor becomes diamagnetic and the flux lines are expelled from the superconductor, resulting in a negative susceptibility. If the pinning interactions in the superconductor become effective as the temperature decreases, flux lines will be prevented from leaving the superconductor, and the susceptibility will be influenced by the pinning. That is, the susceptibility is proposed to be small for a strongly pinned superconductor. Thus, the result does not reflect correctly the volume fraction of superconducting material.

For a description by the critical state model, it is assumed that a magnetic field H_e is applied parallel to a very wide superconducting slab ($0 \leq x \leq 2d$). From sym-

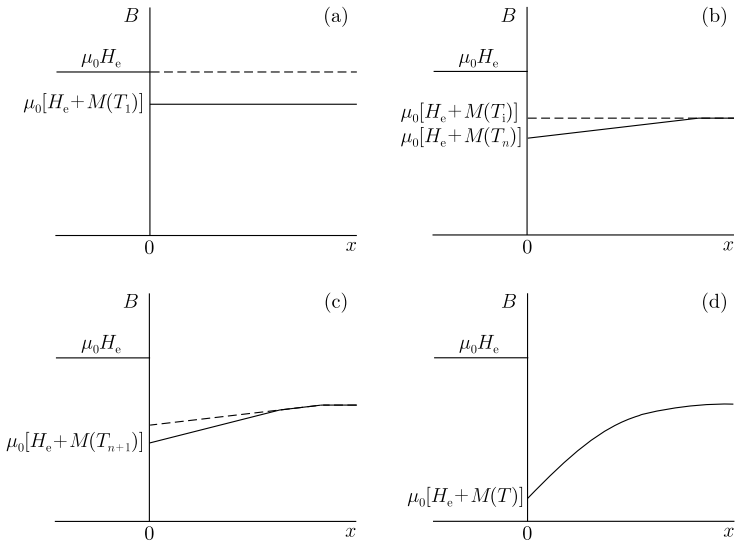

Fig. 3.28 Magnetic flux distribution in a superconductor in the field cooled process (**a**) for $T_1 \le T \le T_c'$, (**b**) when the temperature is decreased slightly by ΔT from T_1, (**c**) when the temperature is further decreased and (**d**) at sufficiently low temperatures

metry we need to treat only half of the slab, $0 \le x \le d$. The critical temperature in the magnetic field H_e is denoted by T_c'. When the temperature T is higher than T_c', the magnetic flux density in the superconductor is uniform and given by $B = \mu_0 H_e$. When the temperature is slightly decreased from T_c' to $T_1 = T_c' - \Delta T$, the superconductor becomes diamagnetic. If T_1 is higher than the irreversibility temperature, $T_i(H_e)$, the pinning does not yet work, and the internal magnetic flux distribution is as schematically shown in Fig. 3.28(a), where $M(< 0)$ is the magnetization. When the temperature is further reduced to $T_n = T_i(H_e) - \Delta T$, the pinning interaction becomes effective. If the critical current density at this stage is denoted by ΔJ_c, the magnetic flux distribution inside the superconducting slab is expected to be like the one shown in Fig. 3.28(b), where the slope of the magnetic flux distribution near the surface is equal to $\mu_0 \Delta J_c$. When the temperature is further decreased, the diamagnetism of the superconductor becomes stronger and the flux lines near the surface are driven to the outside of the superconductor. At the same time the pinning also becomes stronger, and the flux distribution shown in Fig. 3.28(c) results. Thus, the magnetic flux distribution at a sufficiently low temperature is expected to be like that in Fig. 3.28(d).

Here the magnetic flux distribution is calculated analytically. For simplicity the diamagnetic property of the superconductor is approximated as shown in Fig. 3.29. That is, if the temperature at which H_e is equal to the lower critical field H_{c1} is denoted by T_{c1}, the magnetization is given by

$$M(T) = -\epsilon\left[H_{c2}(T) - H_e\right] \tag{3.76}$$

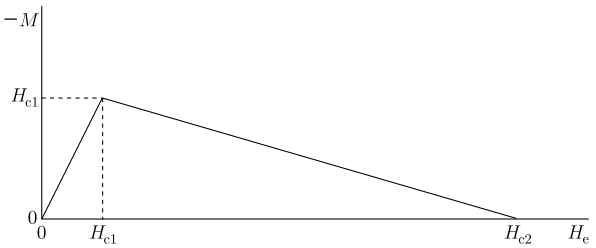

Fig. 3.29 Approximate diamagnetism of a superconductor

for temperatures higher than T_{c1} and by

$$M(T) = -H_e \tag{3.77}$$

for temperatures lower than T_{c1}. In the above the parameter ϵ is given by

$$\epsilon = \frac{H_{c1}}{H_{c2} - H_{c1}}. \tag{3.78}$$

If the temperature dependence of κ is neglected, this parameter does not depend on the temperature. Correctly speaking, this parameter should be given by $\epsilon = 1/1.16(2\kappa^2 - 1)$ in the vicinity of H_{c2}, but the above approximation is used to simplify the analysis. The temperature dependence of H_{c2} is also approximated by

$$H_{c2}(T) = H_{c2}(0)\left(1 - \frac{T}{T_c}\right). \tag{3.79}$$

In addition, the critical current density is assumed to be a function only of the temperature as

$$J_c(T) = A\left(1 - \frac{T}{T_i}\right)^{m'} \tag{3.80}$$

for sufficiently low H_e. If the irreversibility temperature T_i is approximately given by the critical temperature T_c', we have

$$T_i = (1 - \delta)T_c \tag{3.81}$$

with $\delta = H_e/H_{c2}(0)$.

The magnetic flux distribution near the surface of the superconductor is determined only by M and J_c at a given temperature as

$$B(x) = \mu_0 H_e + \mu_0 M(T) + \mu_0 J_c(T)x. \tag{3.82}$$

In general m' is larger than 1. Thus, the history of magnetic flux distribution at higher temperatures remains in the superconductor as shown in Fig. 3.28(d). Namely, the internal flux distribution is equal to the envelope of (3.82) at higher

temperatures in the past. If the region in which the magnetic flux distribution is expressed by (3.82) is $0 \le x \le x_0$, x_0 is obtained from

$$\frac{\partial B(x_0)}{\partial T} = 0 \tag{3.83}$$

at temperatures above T_{c1}. Under the assumptions of (3.76) and (3.79)–(3.81) we have

$$x_0 = \frac{\epsilon[H_{c2}(0) - H_e]}{Am'}\left[1 - \frac{T}{(1-\delta)T_c}\right]^{1-m'}. \tag{3.84}$$

This depth is $x_0 = \infty$ at $T = T_1$ and decreases with decreasing temperature. The envelope of the flux distribution in the internal region can be derived by substituting the obtained x_0 into (3.82). We have only to eliminate T in (3.82) in terms of $x_0(T)$ in (3.84). Then, replacing x_0 by x, the flux distribution in the envelope region is given by

$$B(x) = \mu_0 H_e - \left(m' - 1\right)\mu_0\left[\frac{\epsilon H_{c2}(0)(1-\delta)}{m'}\right]^{m'/(m'-1)}(Ax)^{-1/(m'-1)}. \tag{3.85}$$

This holds within the region $x_0 \le x \le d$.

If the external magnetic field H_e is sufficiently small, the temperature T_{c1} at which H_{c1} is equal to H_e exists. Below this temperature M is given by (3.77), and B just inside the surface is zero. Hence, the magnetic flux distribution at temperatures lower than this remains unchanged. Strictly speaking, the flux lines near the surface are continuously expelled from the superconductor with the strengthened diamagnetism from decreasing temperature as discussed in Sect. 2.6, and hence, the flux distribution does not remain completely unchanged. However, the remaining flux distribution is the "heritage" of distributions at higher temperatures, and hence, its gradient is small and the resultant driving force to expel flux lines from the superconductor is relatively smaller than the pinning force at the ambient temperature. Thus, although this effect increases the diamagnetism slightly, its influence is considered not to be large. The effect of the reversible motion of flux lines, to be discussed in Sect. 3.7, is rather larger than this, since it is considered that the flux lines are likely to be nucleated in the bottom of pinning potentials where the energy is lowest in the field cooled process.

The magnetic flux density and the DC susceptibility can be calculated from the above results. The temperature T_0, at which x_0 is equal to d, is given by

$$T_0 = T_c(1-\delta)\left\{1 - \left[\frac{\epsilon H_{c2}(0)(1-\delta)}{Am'd}\right]^{1/(m'-1)}\right\}. \tag{3.86}$$

After a simple but long calculation we have [34]

$$\chi = \epsilon - \frac{\epsilon}{\delta}\left(1 - \frac{T}{T_c}\right) + \frac{Ad}{2H_e}\left[1 - \frac{T}{(1-\delta)T_c}\right]^{m'}; \quad T_i \ge T > T_0, \tag{3.87a}$$

$$= -\frac{[\epsilon H_{c2}(0)(1-\delta)]^2}{2m'(2-m')dAH_e}\left[1-\frac{T}{(1-\delta)T_c}\right]^{2-m'} + \frac{(m'-1)^2}{(2-m')(Ad)^{1/(m'-1)}H_e}\left[\frac{\epsilon H_{c2}(0)(1-\delta)}{m'}\right]^{m'/(m'-1)}; \quad T_0 \geq T > T_{c1}, \tag{3.87b}$$

$$= -\frac{[\epsilon H_{c2}(0)(1-\delta)]^{m'}}{2m'(2-m')dAH_e^{m'-1}} + \frac{(m'-1)^2}{(2-m')(Ad)^{1/(m'-1)}H_e}\left[\frac{\epsilon H_{c2}(0)(1-\delta)}{m'}\right]^{m'/(m'-1)} \equiv \chi_s; \quad T_{c1} \geq T, \tag{3.87c}$$

where χ_s is the saturated susceptibility at sufficiently low temperatures. The above results are useful for $m' \neq 2$. Calculate the susceptibility also for the case of $m' = 2$ (Exercise 3.5).

Calculated results [34] of DC susceptibility in the field cooled process for various values of A are shown in Fig. 3.30. The DC susceptibility when the temperature is increased in a fixed magnetic field is also shown for comparison. With increasing A, i.e., strengthening pinning force, the susceptibility in the field cooled process takes a smaller negative value, but a larger negative value in the process of increasing temperature in a fixed magnetic field. This can be understood, since the motion of flux lines is more restricted by the stronger pinning force. Figure 3.31 shows the relation between the saturated susceptibility and the size of the superconducting specimen [34]. It turns out that the diamagnetism becomes stronger with decreas-

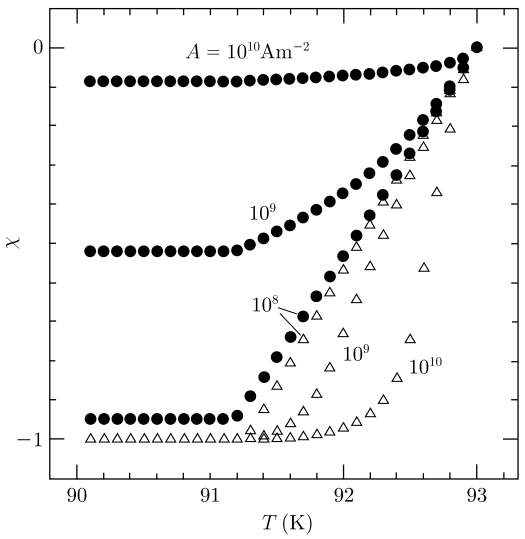

Fig. 3.30 Results of calculated DC susceptibilities for various values of A representing the flux pinning strength in the field cooled process (● ●) and when the temperature is increased in a constant magnetic field (△△) [34]. Assumed parameters are $T_c = 93$ K, $\mu_0 H_{c2}(0) = 100$ T, $\epsilon = 5.13 \times 10^{-4}$, $m = 1.8$, $d = 1$ mm and $\mu_0 H_e = 1$ mT

ing specimen size. This is because the internal flux lines can more easily leave the superconductor when the superconductor is smaller.

The above various results can be qualitatively explained from the magnetic flux distribution in Fig. 3.28. Figure 3.32 shows the dependence of the saturated susceptibility on the external magnetic field for a single crystal specimen of La-based superconductor [34], and the experimental results agree with the above theoretical predictions of the critical state model.

It is assumed here that the superconducting volume fraction is 100 %. However, the obtained saturated susceptibility differs greatly depending on the conditions as

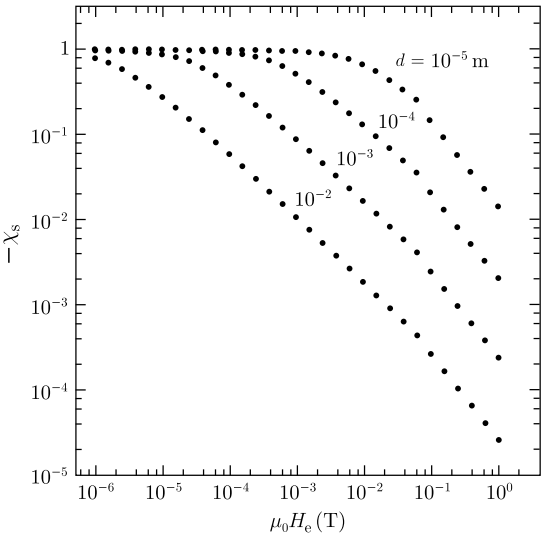

Fig. 3.31 Dependence of saturated DC susceptibility on external magnetic field for various sizes of superconductor [34]. Assumed parameters are $A = 1.0 \times 10^{10}$ A m^{-2} and the same values of T_c, $\mu_0 H_{c2}(0)$, ϵ and m' as in Fig. 3.30

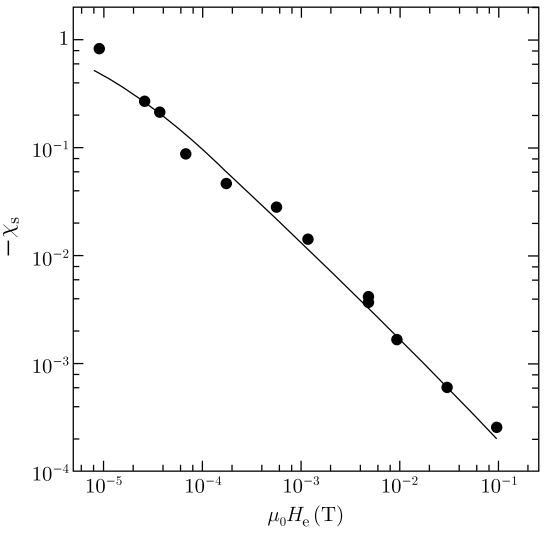

Fig. 3.32 Magnetic field dependence of saturated DC susceptibility of a La-based superconducting specimen [34]. The *solid line* is the theoretical result for $T_c = 35$ K, $\mu_0 H_{c2}(0) = 27.3$ T, $\epsilon = 5.1 \times 10^{-4}$, $A = 8.0 \times 10^{10}$ A m^{-2} and $m' = 1.8$

shown in Figs. 3.30 and 3.31. Hence, this measurement technique is not suitable for evaluation of the superconducting volume fraction.

3.7 Reversible Flux Motion

Most electromagnetic properties of superconductors are irreversible and can be well described in terms of the critical state model. The irreversibility stems from the interaction of flux lines and the pins, i.e., the instability of flux lines as they drop into and jump out of the pinning potential, as discussed in Sect. 2.3. However, if the displacement of flux lines is so small that the flux motion is restricted to the interior of the pinning potential, the corresponding electromagnetic phenomena are expected to become reversible and hence deviate from the critical state description.

Here we assume that the flux lines in some region are in an equilibrium state inside an averaged pinning potential. When the flux lines are displaced by a distance u from the equilibrium position in response to a change of the external magnetic field etc., the pinning potential felt by the flux lines within a unit volume is of the form $\alpha_{\mathrm{L}}u^2/2$, where α_{L}, a constant, is called the Labusch parameter. Hence, the force on the flux lines per unit volume is

$$F = -\alpha_{\mathrm{L}}u, \tag{3.88}$$

which depends only on the position of flux lines u and is reversible. Note the difference between this force and that based on the critical state model according to which the force takes on only one of two values, $\pm J_{\mathrm{c}}B$, depending on the direction of the flux motion. If now b represents the variation in the magnetic flux density due to the movement of flux lines from their equilibrium positions (we assume that the flux movement occurs along the x-axis), using the continuity (2.15) we have

$$\frac{\mathrm{d}u}{\mathrm{d}x} = -\frac{b}{B}, \tag{3.89}$$

where B is an equilibrium value of the magnetic flux density. The Lorentz force that arises from this variation is

$$F_{\mathrm{L}} = -\frac{B}{\mu_0}\cdot\frac{\mathrm{d}b}{\mathrm{d}x}. \tag{3.90}$$

Solutions for u and b can be obtained from the balance between the Lorentz force and the pinning force given by (3.88), $F_{\mathrm{L}} + F = 0$, under given boundary conditions. That is, eliminating u from (3.88)–(3.90), we have

$$\frac{\mathrm{d}^2b}{\mathrm{d}x^2} = \frac{\mu_0\alpha_{\mathrm{L}}}{B^2}b \tag{3.91}$$

and hence,

$$b(x) = b(0)\exp\left(-\frac{x}{\lambda_0'}\right). \tag{3.92}$$

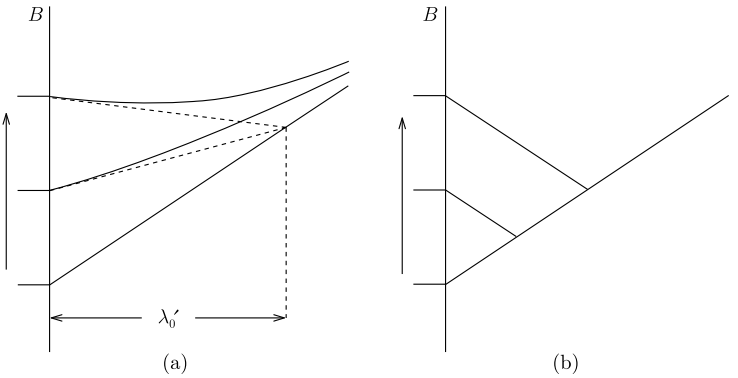

Fig. 3.33 Variations in the magnetic flux distribution in a superconductor when the external magnetic field is increased from the critical state in a decreasing field: (**a**) the case of noticeable reversible motion of flux lines and (**b**) the prediction of the critical state model

In the above the superconductor is assumed to occupy $x \geq 0$, $b(0)$ is a value of b at the surface, $x = 0$, and

$$\lambda_0' = \frac{B}{(\mu_0 \alpha_{\mathrm{L}})^{1/2}}. \tag{3.93}$$

λ_0' is a length called Campbell's AC penetration depth [35]. A solution of the same form can also be obtained for the displacement, $u(x)$. The variation in the magnetic flux density given by (3.92) is similar to (1.14) representing the Meissner effect. This is the reason for referring to λ_0' as a "penetration depth." According to the above solution, the depth to which the variation penetrates is given by λ_0' and is independent of the variation in the magnetic flux density at the surface $b(0)$, for $b(0)$ below some value.

The reversible phenomenon appears for example when the applied field changes from decreasing to increasing. Hence, the initial condition just before the appearance of the reversible phenomenon is mostly the critical state. The variation in the magnetic flux distribution after the field changes from decreasing to increasing is schematically shown in Fig. 3.33(a). On the other hand, based on the critical state model, the distribution would change according to $b(x) = b(0) - 2\mu_0 J_{\mathrm{c}} x$. In this case the depth to which the variation penetrates is $b(0)/2\mu_0 J_{\mathrm{c}}$ and increases in proportion to $b(0)$ (see Fig. 3.33(b)). Thus, the variation in the magnetic flux distribution is different between the reversible and completely irreversible states.

According to experiments, the pinning force density changes from $J_{\mathrm{c}}B$ to $-J_{\mathrm{c}}B$ or inversely (see Fig. 3.34), as the magnetic flux distribution changes as shown in Fig. 3.33(a). That is, the pinning force density varies linearly with u and the phenomenon is reversible as described above, while the displacement u from the initial condition is small. As the mean displacement of the flux lines increases, some flux lines jump out of individual pinning potentials locally and the characteristics of pinning force density vs. displacement vary gradually from reversible to irreversible. When the displacement increases further, the pinning force density ap-

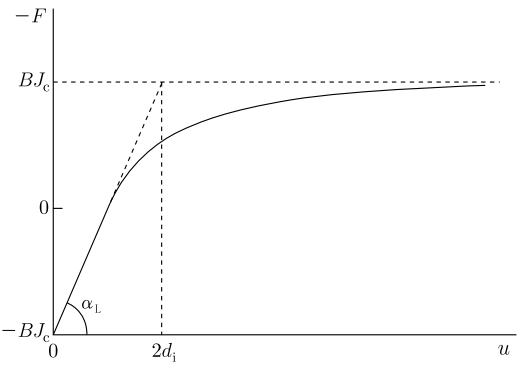

Fig. 3.34 Variation of the pinning force density vs. the displacement of flux lines. Origin is the critical state and the figure shows the characteristics when the flux lines are displaced reversely

proaches asymptotically $-J_c B$ and the phenomenon becomes describable by the irreversible critical state model. Measurements of AC penetration depth λ_0' and the characteristics of pinning force density vs. displacement shown in Fig. 3.34 may be carried out using Campbell's method described in Sect. 5.3.

In practice (see Figs. 3.33(a) and 3.34), the absolute value of the pinning force density is actually given by $F = -\alpha_L u + J_c B$ rather than (3.88) in the reversible region where u is sufficiently small. On the other hand, b is a variation of the magnetic flux density from the initial condition, and hence the Lorentz force is given by $F_L = -(B/\mu_0)(\mathrm{d}b/\mathrm{d}x) - J_c B$. From the balance between the two forces the solution of (3.92) is again obtained.

Here we shall estimate the AC loss in the vicinity of the reversible region. We assume that a DC magnetic field H_e and an AC one of amplitude h_0 are applied parallel to an infinite superconducting slab of thickness $2D$ $(0 \le x \le 2D)$. From symmetry we treat only the half-region, $0 \le x \le D$. If h_0 is sufficiently small, the critical current density J_c can be regarded as a constant. We assume that the initial magnetic flux distribution at the surface field of $H_e - h_0$ is in the critical state and that the variation from this distribution is as shown in Fig. 3.35. The variation in the magnetic flux density from the initial state is again denoted by $b(x)$. Campbell [35] expressed the variation of pinning force density with displacement in Fig. 3.34 as

$$F = -J_c B\left[1 - 2\exp\left(-\frac{u}{2d_i}\right)\right] \tag{3.94}$$

and we go on to make the approximation as $B \simeq \mu_0 H_e$. d_i is half of the displacement when the linear extrapolation of the pinning force density in the reversible regime reaches $J_c B$ in the opposite critical state. That is, d_i represents a radius of the averaged pinning potential and for this reason is referred as the "interaction distance." From the relation

$$J_c B = \alpha_L d_i \tag{3.95}$$

with (3.93) we have

$$d_i = \frac{\mu_0 J_c \lambda_0'^2}{B}. \tag{3.96}$$

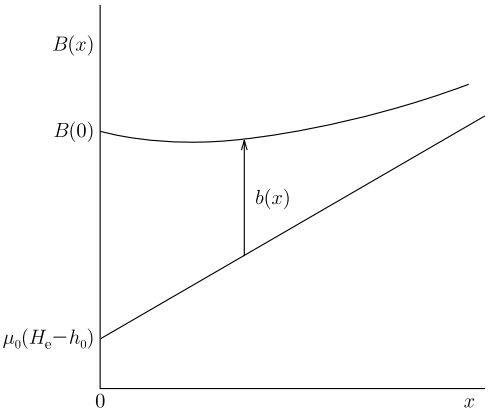

Fig. 3.35 Variation of the magnetic flux distribution in a superconductor when the surface field is increased from $H_e - h_0$ in the critical state

Elimination of u from the force balance equation using (3.89) leads to

$$\frac{d^2b}{dx^2} - \frac{b}{\lambda_0'^2}\left(1 + \frac{1}{2\mu_0 J_c}\cdot\frac{db}{dx}\right) = 0. \tag{3.97}$$

From symmetry the condition $u(D) = 0$ should be satisfied. This is written as $F(D) = J_c B$ or

$$\left.\frac{db}{dx}\right|_{x=D} = 0. \tag{3.98}$$

Equation (3.97) is only numerically solved under this condition and the boundary condition of $b(0)$ at the surface. When the external magnetic field is increased to $H_e + h_0$ and then decreased to $H_e - h_0$, the magnetic flux distribution does not go back to the initial condition. Hence, strictly speaking, it is necessary to obtain the distribution in the steady state after many periods of AC field to estimate the AC loss observed usually. However, this is not easily done and we shall approximate for simplicity that the curve of averaged magnetic flux density vs. external field is symmetric between the increasing and decreasing field processes. In which case, after one period, the last point of the $\langle B\rangle$-H curve meets the initial point and the loop closes. In this way, the AC loss can be estimated approximately. Here it should be noted that the AC loss can be obtained not only from the area of the $\langle B\rangle$-H curve but also from the area of the closed F-u curve as shown in Fig. 3.36. In the latter case, the F-u curve is believed to be approximately symmetric between O $\rightarrow$ A and A $\rightarrow$ O [35].

Figure 3.37 shows the AC losses observed for a bulk Nb-Ta specimen [36], along with the result of theoretical analysis using the Campbell model and with a critical state prediction based on (2.80) and the assumption $\gamma = 1$. According to these results, the difference between the Campbell model and the critical state model is small even when the AC field amplitude is small and hence when the flux motion should be almost reversible; hence it is not clear which model better explains the experimental result. It is, however, possible to distinguish between the two models

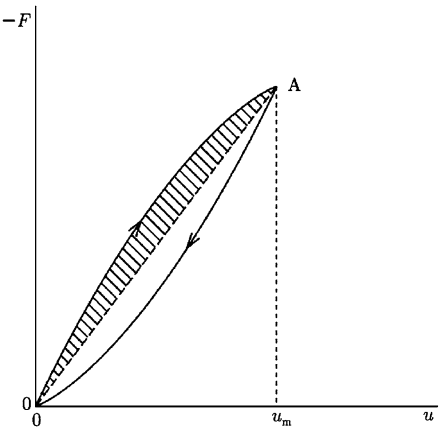

Fig. 3.36 Hysteresis loop of the pinning force density vs. displacement of the flux lines in one cycle of the AC magnetic field

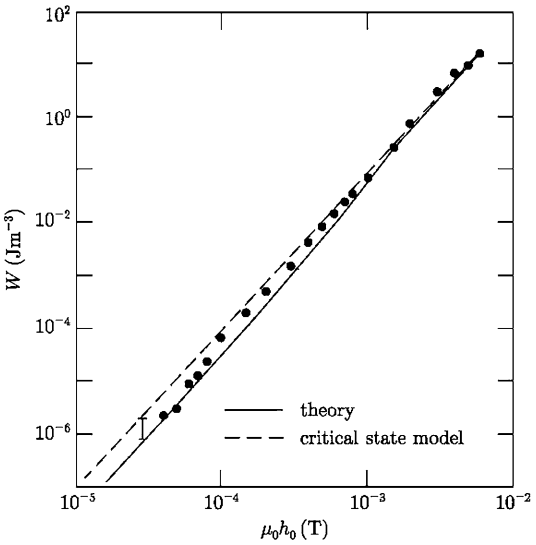

Fig. 3.37 AC energy loss density in a bulk Nb-Ta specimen [36] in a DC bias field $\mu_0 H_e = 0.357$ T. The *solid* and *broken lines* represent the theoretical predictions of the Campbell model and the critical state model, respectively

in terms of the "power factor," which is generally given by

$$\eta_p = \left[1 + \left(\frac{\mu'}{\mu''}\right)^2\right]^{-1/2}, \tag{3.99}$$

where μ' and μ'' are the real and imaginary parts of the fundamental AC permeability, respectively. If we express the time variation of external magnetic field as $h_0 \cos \omega t$, these are written as

$$\mu' = \frac{1}{\pi h_0} \int_{-\pi}^{\pi} \langle B \rangle \cos \omega t \, \mathrm{d}\omega t, \tag{3.100}$$

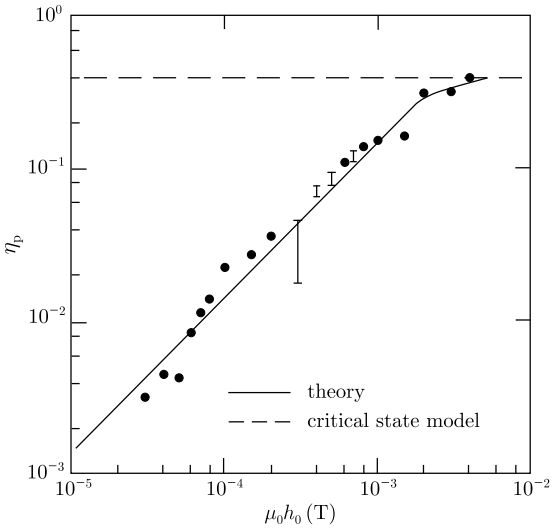

Fig. 3.38 Power factor of AC energy loss density in a bulk Nb-Ta specimen [36] shown in Fig. 3.37. The *solid* and *broken lines* represent the theoretical predictions of the Campbell model and the critical state model, respectively

$$\mu'' = \frac{1}{\pi h_0} \int_{-\pi}^{\pi} \langle B \rangle \sin \omega t \, \mathrm{d}\omega t. \tag{3.101}$$

The AC energy loss density, W, is related to the imaginary AC permeability μ'' through

$$W = \pi \mu'' h_0^2. \tag{3.102}$$

According to the critical state model with $\gamma = 1$ (the Bean-London model) (3.99) reduces to

$$\eta_\mathrm{p} = \left[1 + \left(\frac{3\pi}{4} \right)^2 \right]^{-1/2} \simeq 0.391, \tag{3.103}$$

which is independent of h_0. The observed power factor for the Nb-Ta specimen and the predictions of the two models are compared in Fig. 3.38. It is found from this figure that the phenomenon is well explained by the Campbell model in which the effect of reversible flux motion is taken into account, while the prediction of the critical state model deviates from the experiment. η_p is proportional to h_0 in the region of small h_0. The derivation of η_p predicted by the Campbell model is Exercise 3.8.

As is seen from Fig. 3.37, the AC loss itself in a bulk superconductor is close to the prediction of the critical state model. This is the reason why the reversible effect has not been noticed. Why is the AC loss close to the prediction of the irreversible critical state model? In the regime of almost reversible flux motion, the displacement u is sufficiently small and the pinning force density in (3.94) can be approximately expanded in a power series in u:

$$F = J_\mathrm{c} B \left[1 - \frac{u}{d_\mathrm{i}} + \left(\frac{u}{2d_\mathrm{i}} \right)^2 \right]. \tag{3.104}$$

Here F increases with increasing u as in the upper curve of Fig. 3.36 and the area of the hatched region gives a half of the energy loss density in one period of AC field. Hence, the irreversible component in F is a deviation from the linear line connecting the origin O and the point A. After a simple calculation we have

$$F_{\mathrm{irr}} = -\frac{J_{\mathrm{c}}B}{4d_{\mathrm{i}}^2}\left(u_{\mathrm{m}}u - u^2\right), \tag{3.105}$$

where $u_{\mathrm{m}}(x)$ is the maximum displacement. Here we shall estimate the displacement. Since the flux motion is almost reversible, the penetration of the AC flux can be approximated by (3.92). From (3.89) we have

$$u(x) = \frac{b(0)\lambda_0'}{B}\exp\left(-\frac{x}{\lambda_0'}\right), \tag{3.106}$$

where $b(0)$ is the variation in the magnetic flux density at the surface from the initial condition. $u_{\mathrm{m}}(x)$ is given by this equation with a replacement of $b(0)$ by $2\mu_0 h_0$. Hence, the energy loss density during the variation in $b(0)$ by $\mathrm{d}b(0)$ is given by $-F_{\mathrm{irr}}\mathrm{d}u$ with $\mathrm{d}u$ denoting the variation in u in this period and is written as

$$\mathrm{d}w = \frac{J_{\mathrm{c}}\lambda_0'^3}{4d_{\mathrm{i}}^2B^2}\exp\left(-\frac{3x}{\lambda_0'}\right)\left[2\mu_0 h_0 b(0) - b^2(0)\right]\mathrm{d}b(0). \tag{3.107}$$

Since $b(0)$ varies from 0 to $2\mu_0 h_0$ in a half period, the energy loss density is calculated to be

$$W = \frac{2}{D}\int_0^{2\mu_0 h_0}\mathrm{d}b(0)\int_0^D \mathrm{d}x\cdot\frac{\mathrm{d}w}{\mathrm{d}b(0)} = \frac{2\mu_0 h_0^3}{9J_{\mathrm{c}}D}. \tag{3.108}$$

In the above we assumed that $D \gg \lambda_0'$. This value is 1/3 of the prediction of the critical state model. The reason for the relatively small difference is that the displacement and the region in which the loss occurs are enhanced, while the irreversible force density $|-F_{\mathrm{irr}}|$ is decreased, resulting in an approximate offset.

The reversible phenomenon does not affect the electromagnetic property appreciably for a bulk superconductor sufficiently thicker than λ_0'. However, it is considered from a comparison between (a) and (b) in Fig. 3.33 that reversibility will become noticeable for a superconductor with the size comparable to or smaller than λ_0'. λ_0' is of the order of 0.5 μm at 1 T in a superconductor with the flux pinning strength comparable to a commercial Nb-Ti wire; accordingly the reversible phenomenon is really noticeable [37] in multifilamentary wires for AC use which have superconducting filaments thinner than the above value. As a result the dependence of the AC loss on the filament diameter shows a departure from the critical state prediction. That is, the critical state model predicts that the breaking point of the loss curve should shift to smaller AC field amplitudes accompanied by increasing loss in the lower amplitude region with decreasing filament diameter (see inset of Fig. 3.39) in complete conflict with the experimental result. On the other hand, in the region of large AC field amplitudes, the loss agrees with the prediction of the critical state

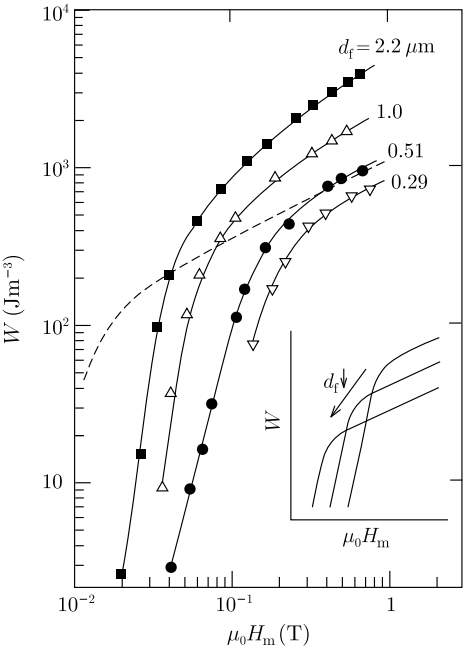

Fig. 3.39 AC energy loss density in a multifilamentary Nb-Ti wires with very fine filaments [37]. H_m is an AC magnetic field amplitude and a DC bias field is not applied. The *broken line* shows the prediction of the critical state model with the observed critical current density for filament diameter 0.51 μm. *Inset* represents the prediction of the critical state model on the variation of AC energy loss density with the filament diameter

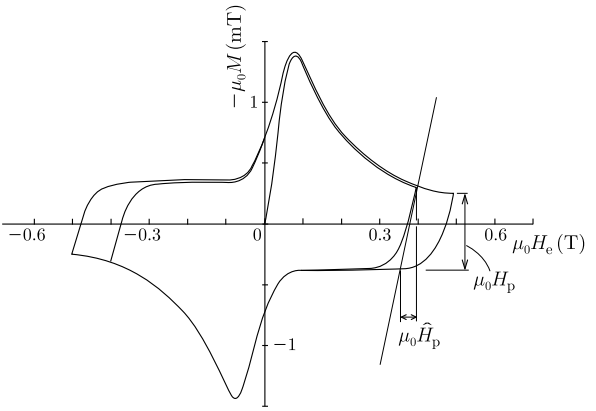

Fig. 3.40 Magnetization curve for a Nb-Ti multifilamentary wire [37] of filament diameter 0.51 μm

model. Another result is that the slope of the minor magnetization curve when the sweep of magnetic field is changed from increasing to decreasing takes on a much smaller value than theoretically predicted, i.e., it is 1 for a large slab in a parallel field and 2 for a cylinder in a perpendicular field, as shown in Fig. 3.40 (note a difference in scales between the ordinate and the abscissa). This slope becomes smaller with increasing magnetic field.

Such an abnormal phenomenon originates from the reversible flux motion. Usually the filament diameter d_f is not sufficiently greater than the flux line spacing a_f. For instance, at $B = 1$ T a_f is 49 nm and hence only ten rows of flux lines exist

in a filament of diameter 0.5 μm. Hence, the applicability of the semimacroscopic Campbell model to the macroscopic description of the spatial variation of magnetic flux distribution is in doubt. However, in the usual specimens the number of filaments is very large and the dimension along the length of the filament is also large. The magnetic quantity usually observed is the average within a large number of long filaments and hence the semimacroscopic description is considered to be possible only as an averaged flux distribution. The local flux distribution is expected to be different from such an averaged one. This is also the case in a bulk superconductor and even in the critical state. That is, it is not correct to postulate that the local flux distribution is of uniform slope equal to $\mu_0 J_c$ in the critical state of a bulk superconductor. In fact, the slope may take on various values locally and $\mu_0 J_c$ is nothing other than the average value. The fact that the critical state model holds for multifilamentary wires with many filaments and sufficient length has been validated by many experiments. This does not contradict the above speculation that the semimacroscopic description is possible for the averaged distribution. Hence, the Campbell model is considered to be applicable to multifilamentary superconducting wires even with very fine filaments.

Takács and Campbell [38] calculated the AC loss in a wire with very fine superconducting filaments in a small AC magnetic field of amplitude h_0 superposed to DC field. They assumed that the magnetic flux penetrates uniformly the very fine superconducting filaments. The filament of diameter d_f was approximated by a slab of thickness d_f. Here we shall calculate the AC loss using (3.104) in a different manner from [38]. Only the half, the region $0 \le x \le d_f/2$ is considered. The displacement of flux lines in this region is obtained from (3.89) as

$$u(x) = \frac{b(0)}{B}\left(\frac{d_f}{2} - x\right), \tag{3.109}$$

where the symmetry condition, $u = 0$ at the center, $x = d_f/2$, was used. The loss in this case can also be estimated by substituting (3.109) into (3.105) as done previously; u_m is again given by (3.109) with $b(0)$ replaced by $2\mu_0 h_0$. D is replaced by $d_f/2$ in (3.108), and after some calculation we have

$$W = \frac{\mu_0 h_0^3}{3 J_c d_f}\left(\frac{d_f}{2\lambda_0'}\right)^4. \tag{3.110}$$

This agrees with the result of Takács and Campbell [38] and is $(d_f/2\lambda_0')^4/4$ times as large as the prediction of the Bean-London model. Thus, the loss decreases rapidly with decreasing filament diameter. It is concluded that the reversible effect is very large in small superconductors for the following reason. Because of symmetry, the flux lines in the center of the filament do not move and are restrained around the origin of the pinning force vs. displacement curve shown in Fig. 3.34. The average displacement of flux lines is approximately proportional to the filament diameter, and hence, most of the flux lines in the filament are in the reversible regime.

When the AC field amplitude becomes large, the loss approaches asymptotically $2\mu_0 H_p h_0$, where $H_p = J_c d_f/2$ is the penetration field (see (2.84)). From the intersecting point between this relationship and the extrapolation of (3.110), the breaking point of the loss curve shown in Fig. 3.39 is

$$\widetilde{H}_p = 2\sqrt{3}\left(\frac{2\lambda_0'}{d_f}\right)^2 H_p = 4\sqrt{3}\frac{J_c\lambda_0'^2}{d_f}. \tag{3.111}$$

Hence, the breaking point shifts to higher AC field amplitudes with decreasing filament diameter. Thus, the dependence of the loss on the filament diameter obeys the Campbell description of reversible phenomenon. In the irreversible Bean-London model $\widetilde{H}_p = \sqrt{3}H_p$.

Suppose we extrapolate the tangent to the minor magnetization curve in Fig. 3.40, then the magnetic field variation needed to reach the opposite major curve is represented by $\widehat{H}_p$, which is called the apparent penetration field. According to the Campbell model the slope of the minor magnetization curve, $H_p/\widehat{H}_p$, is a function only of $d_f/2\lambda_0'$ and given by [37]

$$\frac{H_p}{\widehat{H}_p} = 1 - \frac{2\lambda_0'}{d_f}\tanh\left(\frac{d_f}{2\lambda_0'}\right), \tag{3.112}$$

where the slab approximation is used. In the extreme reversible case in which $d_f/2\lambda_0' \ll 1$ is satisfied, we have $\widehat{H}_p = (\sqrt{3}/2)\widetilde{H}_p = 3(2\lambda_0'/d_f)^2 H_p$. On the other hand, in the case where the Bean-London model holds and $d_f/2\lambda_0' \gg 1$, $\widehat{H}_p$ coincides with H_p. Because of demagnetization the slope of the minor magnetization curve takes on double the value given by (3.112) for multifilamentary wires in the transverse magnetic field. Figure 3.41 shows the dependences of H_p and $\widehat{H}_p$ on fila-

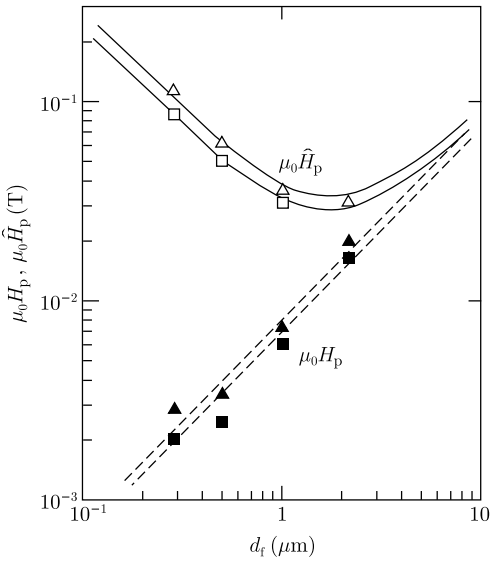

Fig. 3.41 Dependences of the characteristic fields, H_p and $\widehat{H}_p$, on the filament diameter for Nb-Ti multifilamentary wires [37]. *Triangular* and *square symbols* show the values of the characteristic fields for $\mu_0 H_e = 0.40$ T and 0.55 T, respectively. The *solid lines* are $\widehat{H}_p$ estimated from (3.112) with H_p shown by the *broken lines* and the assumptions of $\lambda_0' = 0.56$ μm (0.40 T) and 0.54 μm (0.55 T)

ment diameter d_f for Nb-Ti multifilamentary wires and it is found that these are well described by the Campbell model.

Numerically calculated results of the energy loss density [36] for various filament diameters are shown in Fig. 3.42. In the case of very fine filaments in (a) the result is close to the analytic expression of (3.110) represented by the straight broken lines. The chained lines are the results of the irreversible Bean-London model. The numerical result tends to approach the prediction of this model as the filament diameter increases.

The AC energy loss density shown in Fig. 3.39 was observed in the absence of a large DC bias field, which is different from the above condition. In this case (3.89), the approximate formula based on the continuity equation for flux lines does not hold. In addition, not only J_c but also λ_0' depends on the magnetic field strength. Therefore, a rigorous analysis is necessary. However, (3.110) is expected to be qualitatively correct. In practice the observed AC loss in recent multifilamentary wires with ultra fine filaments under small AC field amplitudes is even much smaller than

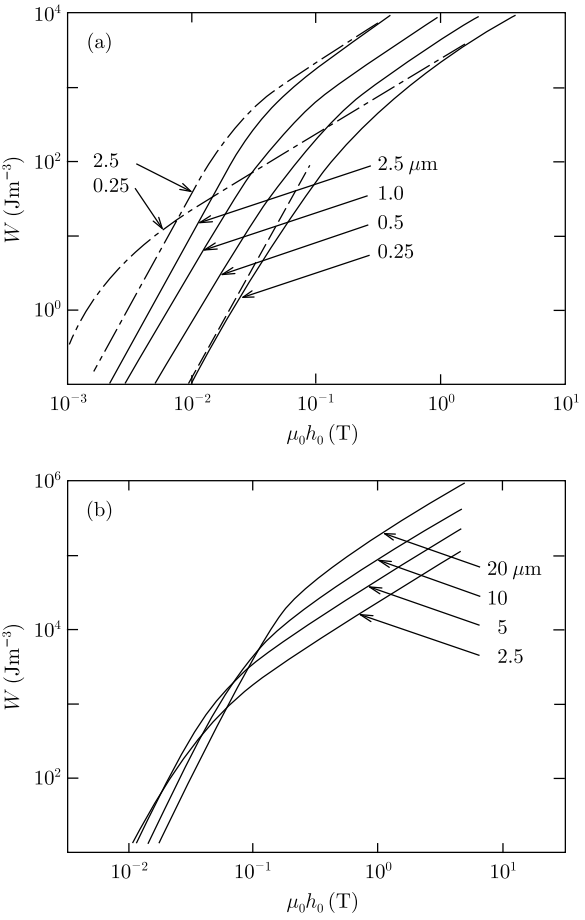

Fig. 3.42 AC energy loss density estimated using the Campbell model for various filament diameters [36]. The *broken* and *chained lines* show the results of (3.110) and the Bean-London model, respectively. Assumed parameters are $J_c = 1.0 \times 10^{10}$ A m^{-2} and $\lambda_0' = 0.63$ μm

the prediction of (3.110). In such wires the diameter of superconducting filaments is comparable to, or smaller than, the London penetration depth and the first penetration field is significantly enhanced as discussed in Appendix A.3. For example, if d_f is not much smaller than the London penetration depth λ, the effective lower critical field is predicted to be

$$H_{c1}^* \simeq \left[1 - \frac{2\lambda}{d_f} \tanh\left(\frac{d_f}{2\lambda}\right)\right]^{-1} H_{c1}. \tag{3.113}$$

From the result of Exercise 2.10, the corresponding energy loss density is given by

$$W = \frac{\mu_0}{3 J_c d_f}\left(\frac{d_f}{2\lambda_0'}\right)^4 \left(H_m - H_{c1}^*\right)^2 \left(H_m + \frac{H_{c1}^*}{2}\right), \tag{3.114}$$

where h_0 is rewritten as H_m.

The AC penetration depth λ_0' defined by Campbell is an important quantity related to the AC loss in multifilamentary wires with very fine filaments. However, this length cannot be measured using Campbell's method in case the filament diameters are smaller than λ_0' (see Exercise 5.3). There are two methods for estimating λ_0' in this case; one is to compare the slope of minor magnetization curve with (3.112) and the other is to analyze the imaginary part of AC susceptibility as will be mentioned in Sect. 5.4.

3.8 Flux Creep

The superconducting current originated from the flux pinning mechanism has been assumed to be persistent in time so long as the external conditions are unchanged. However, if the DC magnetization of a superconducting specimen is measured for a long period, it is found to decrease slightly as shown in Fig. 3.43. That is, the superconducting current supported by the flux pinning is not a true persistent current but decreases with time. This results from the fact that the state in which the flux lines are restrained by the pinning potentials is only a quasistable one corresponding to a local minimum of the free energy in the state space and is not an actual equilibrium state. Therefore, a relaxation to the real equilibrium state, i.e., a decay of the shielding current takes place; it does so logarithmically with time as indicated in Fig. 3.43. The decay of the persistent current is accompanied by a decrease of the slope of the magnetic flux distribution caused by the motion of flux lines. Such flux motion is called "flux creep" which according to Anderson and Kim [39] is caused by thermal activation. It is supposed that thermally activated flux motion is not a macroscopic and continuous phenomenon like flux flow, but a partial and discontinuous one. The group of flux lines that move collectively is called the flux bundle.

We imagine one flux bundle to move under the influence of the transport current. When the flux bundle is virtually displaced in the direction of the Lorentz force, the variation in the energy of the flux bundle will be as shown schematically in Fig. 3.44(a). Point A corresponds to the state in which the flux bundle is pinned,

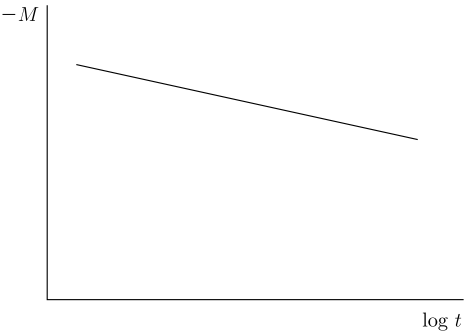

Fig. 3.43 Relaxation of magnetization due to flux creep

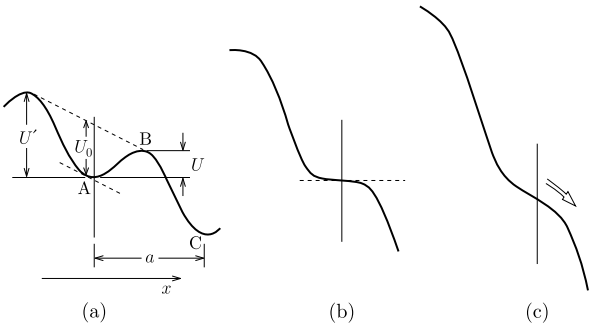

Fig. 3.44 Energy of flux bundle vs. its position: (**a**) the case of transport current less than the virtual critical value. The flux bundle must overcome the barrier U so as to be depinned from the potential. (**b**) the virtual critical state and (**c**) the flux flow state

and the gradual decrease of energy that takes place when the flux bundle moves to the right represents the work done by the Lorentz force. It is necessary for the flux bundle to overcome the energy barrier at point B so as to be depinned. If there is no thermal activation, the state indicated in this figure is stable and the flux bundle does not move. In this virtual case, it is considered that the critical state is attained when the current density is increased until the peak and the bottom of the energy curve coincide with each other as shown in Fig. 3.44(b). At a higher current density continuous flux motion i.e., flux flow is expected to occur as in (c).

At a finite temperature T, thermal activation enables the flux bundle to overcome the energy barrier even in the state represented by Fig. 3.44(a). If the thermal energy, $k_{\mathrm{B}}T$, is sufficiently small compared to the energy barrier, U, where k_{B} is the Boltzmann constant, the probability for the flux bundle to overcome the barrier for each attempt is given by the Arrhenius expression, $\exp(-U/k_{\mathrm{B}}T)$. Hence, if the attempt frequency of the flux bundle is ν_0 and the distance by which the flux bundle moves during one hopping is a, the mean velocity of the flux lines to the right-hand side is given by $a\nu_0 \exp(-U/k_{\mathrm{B}}T)$. The oscillation frequency ν_0 is expressed in terms of the Labusch parameter α_{L} and the viscous coefficient η as [40]

$$\nu_0 = \frac{\phi_0 \alpha_{\mathrm{L}}}{2\pi B \eta}. \tag{3.115}$$

This is the frequency of damped oscillation within the averaged pinning potential. This is seen from the following argument: the relaxation time in the pinning poten-

tial is given as $\tau \sim \eta^*/k_\mathrm{p}$ from (2.41), where k_p, the Labusch parameter per unit pinning center, is given by $k_\mathrm{p} = \alpha_\mathrm{L}/N_\mathrm{p}$ where N_p is the pin concentration; thus, $\nu_0 \simeq 1/2\pi\tau$. In Sect. 2.3 the number of flux lines in the flux bundle is assumed to be 1.

When the flux bundle is displaced by the flux line spacing a_f, its condition is expected to be approximately the same as before the displacement. In other words, the hopping distance a is supposed to be comparable to a_f. In general flux motion towards the left-hand side is also considered, hence the induced electric field according to (2.17) is given by

$$E = Ba_\mathrm{f}\nu_0\left[\exp\left(-\frac{U}{k_\mathrm{B}T}\right) - \exp\left(-\frac{U'}{k_\mathrm{B}T}\right)\right], \tag{3.116}$$

where U' is the energy barrier for the flux motion opposite to the Lorentz force (see Fig. 3.44(a)). Thus, the electric field is generated by the motion of flux lines due to the flux creep. The mechanism responsible for the appearance of the electric field is essentially the same as that for flux flow in spite of the quantitative difference, and hence, a distinction in experiments between flux creep and flow is difficult. According to analysis of experimental results, most of the observed electric field at which the critical current density is determined by the usual four-terminal method comes from the mechanism of flux creep, as will be shown in Chap. 8. Hence, it is necessary to take account of the mechanisms of both flux creep and flow to analyze the practical E-J characteristics. The theoretical model of flux creep and flow used for the analysis of the E-J curves is described in Sect. 8.5.2. The electromagnetic phenomena in high-temperature superconductors will be analyzed using this model, and the results will be discussed in Sect. 8.5.3.

Here we treat for simplicity the magnetic relaxation of a large superconducting slab ($0 \le x \le 2d$) in a magnetic field along the z-axis. From symmetry we need to treat only the half, $0 \le x \le d$. In an increasing field, the current flows along the positive y-axis and the motion of flux lines due to the flux creep occurs along the positive x-axis. If the average current density is denoted by J, the magnetic flux density is $B = \mu_0(H_\mathrm{e} - Jx)$. In terms of its average value $\langle B\rangle$, the electric field at the surface, $x = 0$, is given by the Maxwell equation (2.2) as

$$E = \frac{\partial d\langle B\rangle}{\partial t} = -\frac{\mu_0 d^2}{2}\cdot\frac{\partial J}{\partial t}. \tag{3.117}$$

The relaxation of the superconducting current density with time can be obtained by substituting this equation into the left-hand side of (3.116) with U and U' expressed as functions of J.

Here we shall treat the case where the relaxation of the superconducting current is small in the vicinity of the virtual critical state. In this case $U \ll U'$ and the second term in (3.116) can be neglected. It is clear from Fig. 3.44(a) that U increases with decreasing J. Hence, it is reasonable to express U by expanding it in the form $U = U_0^* - sJ$, where U_0^* is the apparent pinning potential energy in the limit $J \to 0$ and s is a constant. As shown in Fig. 3.44(b) $U = 0$ is attained in the virtual critical state

and the current density in this state is denoted by J_{c0}. Then, we have approximately $s = U_0^*/J_{c0}$ and

$$U = U_0^*\left(1 - \frac{J}{J_{c0}}\right). \tag{3.118}$$

Hence, the equation describing the time variation of the current density is given by

$$\frac{\partial J}{\partial t} = -\frac{2Ba_f\nu_0}{\mu_0 d^2}\exp\left[-\frac{U_0^*}{k_B T}\left(1 - \frac{J}{J_{c0}}\right)\right]. \tag{3.119}$$

This equation is easily solved and under the initial condition that $J = J_{c0}$ at $t = 0$ we obtain

$$\frac{J}{J_{c0}} = 1 - \frac{k_B T}{U_0^*}\log\left(\frac{2Ba_f\nu_0 U_0^* t}{\mu_0 d^2 J_{c0} k_B T} + 1\right). \tag{3.120}$$

After a sufficient time, the 1 in the argument of the logarithm can be neglected and the time variation of the current density shown in Fig. 3.43 can be derived. The apparent pinning potential energy U_0^* can be estimated from the logarithmic relaxation rate:

$$-\frac{\mathrm{d}}{\mathrm{d}\log t}\left(\frac{J}{J_{c0}}\right) = \frac{k_B T}{U_0^*}. \tag{3.121}$$

The energy barrier U is not generally a linear function of J, as in (3.118), over a wide range of J. The relaxation of the current for such a case will be discussed below: we simply approximate the relationship between the energy of the flux bundle and its central position, x, shown in Fig. 3.44(a) as

$$F(x) = \frac{U_0}{2}\sin kx - fx, \tag{3.122}$$

where $k = 2\pi/a_f$ and $f = JBV$ with V denoting the volume of the flux bundle. Differentiating (3.122) with respect to x, the quasiequilibrium position of the flux bundle is obtained:

$$x = -x_0 = -\frac{1}{k}\cos^{-1}\left(\frac{2f}{U_0 k}\right). \tag{3.123}$$

On the other hand, $F(x)$ is locally maximum at $x = x_0$. Hence, the energy barrier is obtained as $U = F(x_0) - F(-x_0)$. That is,

$$\frac{U}{U_0} = \left[1 - \left(\frac{2f}{U_0 k}\right)^2\right]^{1/2} - \frac{2f}{U_0 k}\cos^{-1}\left(\frac{2f}{U_0 k}\right). \tag{3.124}$$

If there is no thermal activation, the virtual critical state with $U = 0$ will be attained. In this case $x_0 = 0$ will be reached, and hence, $2f/U_0 k = 1$ will be satisfied. Since J in this case is equal to J_{c0}, the general relation

$$\frac{2f}{U_0 k} = \frac{J}{J_{c0}} \equiv j \tag{3.125}$$

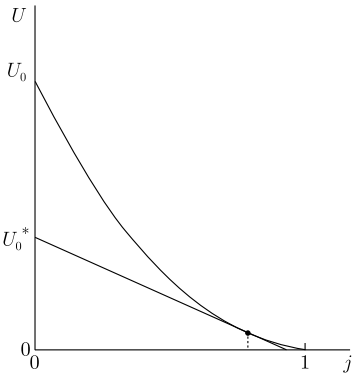

Fig. 3.45 Relationship between the energy barrier U and the normalized current density j. Extending the tangent at a given value of current density to $j = 0$, the intercept gives the apparent pinning potential energy U_0^*

is derived. In terms of the normalized current density j, (3.124) can be written as

$$\frac{U}{U_0} = \left(1 - j^2\right)^{1/2} - j\cos^{-1} j. \tag{3.126}$$

In case j is very close to 1 so that $1 - j \ll 1$, (3.126) reduces to $U/U_0 \simeq (2\sqrt{2}/3)(1-j)^{3/2}$. In this case j is described by

$$\frac{\partial j}{\partial t} = -c\exp\left[-\frac{U(j)}{k_\mathrm{B}T}\right], \tag{3.127}$$

where $c = 2Ba_\mathrm{f}\nu_0/\mu_0 J_{\mathrm{c}0}d^2$. $U(j)$ is strictly a nonlinear function. If we expand $U(j)$ as in (3.118) within a narrow region, the variation of j as in (3.120) will be obtained. However, the value of U_0^* estimated from the relaxation is different from the real pinning potential energy, U_0. That is, U_0^* is usually smaller than U_0 as shown in Fig. 3.45. Hence, the measurement of magnetization relaxation leads to an underestimate of the pinning potential energy.

Here we shall show an example of the numerical analysis. We assume the temperature dependence of the virtual critical current density to be $J_{\mathrm{c}0} = A[1-(T/T_\mathrm{c})^2]^2$. In case of strong pinning, the pinning potential energy U_0 is proportional to $J_{\mathrm{c}0}^{1/2}$ as will be shown in Sect. 7.7. Hence, the temperature dependence of U_0 is given by

$$U_0 = k_\mathrm{B}\beta\left[1 - \left(\frac{T}{T_\mathrm{c}}\right)^2\right], \tag{3.128}$$

where β is a constant dependent on the flux pinning strength. Here we assume an Y-based high-temperature superconductor with $T_\mathrm{c} = 92$ K and other parameters: $B = 0.1$ T ($a_\mathrm{f} = 0.15$ μm), $\nu_0 = 1.0 \times 10^6$ Hz, $d = 1.0 \times 10^{-4}$ m and $A = 3.0 \times 10^9$ A m^{-2}. The results of numerical calculation [41] on the time dependence of j at various temperatures for $\beta = 3000$ K are shown in Fig. 3.46. Figure 3.47(a) shows the apparent pinning potential energy U_0^* obtained from the average logarithmic relaxation rate in the range of $1 \le t \le 10^4$ s according to (3.121). In addition, (b) represents the relationship between U_0 and U_0^* for $\beta = 10000$ K.

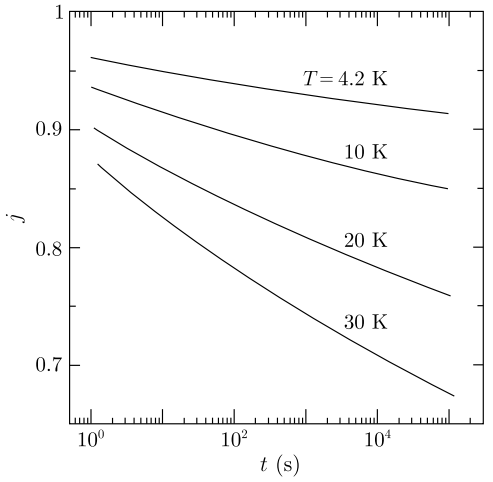

Fig. 3.46 Relaxation of normalized current density [41] obtained from (3.127) in case $\beta = 3000$ K

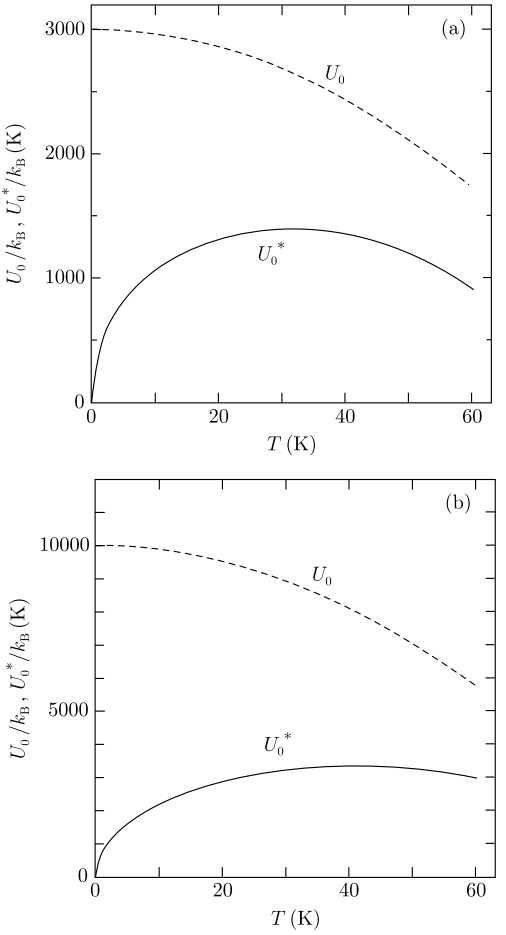

Fig. 3.47 Calculated apparent pinning potential energy U_0^* for given values of U_0 [41] for (**a**) $\beta = 3000$ K and (**b**) $\beta = 10000$ K

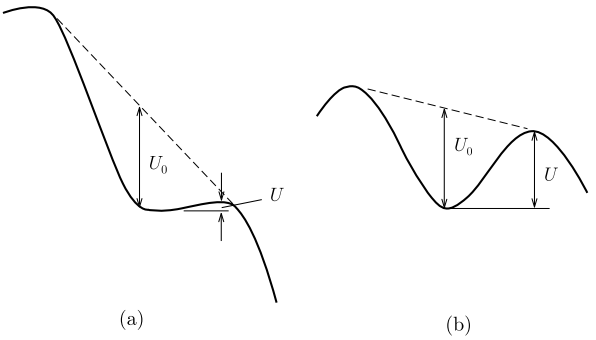

Fig. 3.48 (**a**) Relationship between the energy of flux bundle and its position at measurement of magnetization at low temperatures. Since the relaxation from the virtual critical state is not large, the energy barrier U is small. (**b**) Condition at measurement at high temperatures. Since the relaxation has already taken place to a considerable extent, U is large

It turns out that the U_0^* obtained is much smaller than the given U_0 and the difference becomes larger at lower temperatures, especially in the limit $T \to 0$, U_0^* approaches 0. Furthermore U_0^*/U_0 decreases as U_0 increases. In practice, according to the numerical calculation by Welch [42], if the current dependence of the activation energy is given by $U/U_0 \propto (1-j)^N$, the apparent pinning potential is expressed as (see Exercise 3.11)

$$U_0^* = c_N \left[(k_B T)^{N-1} U_0 \right]^{1/N}. \tag{3.129}$$

In the case of sinusoidal washboard potential discussed above, $N = 3/2$ and $c_{3/2} = 1.65$. This result explains the above behavior exactly.

How can we understand this result? Assume that the initial state at $t = 0$ is the virtual critical state shown in Fig. 3.44(b).[2] The measurement of magnetic relaxation starts some time after the establishment of the initial state, at which time the variation in the energy of the flux bundle vs. its position is shown in Fig. 3.48 for (a) low temperatures and (b) high temperatures. That is, at the low temperature in (a) little relaxation has taken place, and the energy barrier U is small; hence, the flux creep takes place easily, and the apparent pinning potential energy U_0^* is small. On the other hand, in (b) where the temperature is higher, the relaxation has already taken place revealing a large U; in this case, the flux creep is suppressed and the resultant U_0^* is large. This result can also be explained from Fig. 3.45. At low temperatures j at the time of measurement is close to 1 and U_0^* obtained from extrapolating the

[2] In practice, even if we try to instantaneously establish an ideal external condition such as magnetic field before the flux creep starts, the relaxation due to the viscosity shown in Sect. 3.2 is added. Hence, the condition in Fig. 3.44(b) is not realized in a strict sense. However, the results after a sufficient long time do not seem to depend sensitively on the initial condition as usually observed, and the above assumption will be admitted.

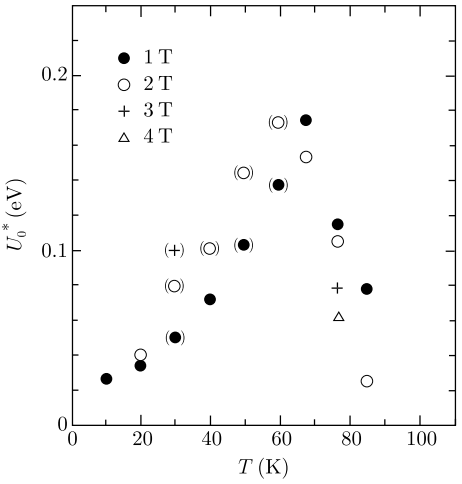

Fig. 3.49 Temperature dependence of apparent pinning potential energy U_0^* obtained from the magnetic relaxation for a melt-processed Y-B-C-O [42]

tangential line is much smaller than U_0. On the other hand, at high temperatures j is small and U_0^* is close to U_0. Furthermore the dependence of U_0^* on U_0 at a constant temperature has a similar explanation. The cases of large and small U_0 correspond qualitatively to Fig. 3.48(a) and (b), respectively.

Figure 3.49 shows some experimental U_0^* data for Y-B-C-O [42]: U_0^* takes on a small value at low temperatures and its temperature dependence agrees qualitatively with the theoretical prediction as in Fig. 3.47. The observed flux creep phenomena can be approximately explained by the model assuming a simple sinusoidal variation in the energy given by (3.122). Flux creep in response to such a spatial variation in the potential was first pointed out by Beasley et al. [43] and later investigated in detail by Welch [42]. It should be noted that the shape of potential around the inflection point has a significant influence on the magnetic relaxation. However, any discussion has not yet been given on this problem in literature. Other mechanisms have also been proposed to explain the temperature dependence of U_0^* shown in Fig. 3.49, such as; the statistical distribution of the pinning potential energy [44], the nonlinear dependence of the energy barrier U on J [45] due to an enlargement of the pinning correlation length, that gives the flux bundle size, with decreasing J, etc. However, the width of distributed pinning potential energy necessary to explain the temperature dependence of U_0^* seems to be much larger than the observed distribution width of the critical current density. As for pinning correlation length enhancement, Campbell's AC penetration depth, as measured using Campbell's method described in Sect. 5.3, is not enhanced in the vicinity of $J = 0$. From these observations and from the fact that the shape of the pinning potential is necessarily involved when the flux bundle overcomes the barrier, it seems natural that the temperature dependence of U_0^* originates mainly from the shape of the pinning potential. However, it is difficult to explain the temperature dependence of U_0^* at low temperature from only the simple effects of the pinning potential shape. This problem will be discussed in Appendix A.9.

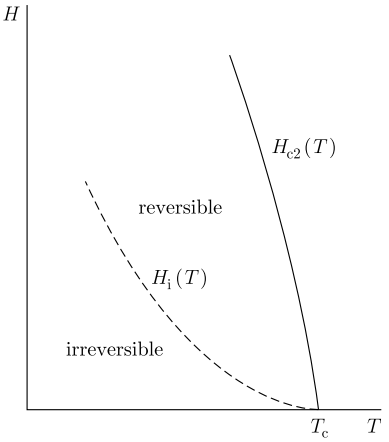

Fig. 3.50 Phase boundary $H_{c2}(T)$ and irreversibility line $H_i(T)$ on the temperature-magnetic field plane

It should be noted that, from the measurement of magnetic relaxation, the actual pinning potential energy that is important to the physics of flux pinning cannot be obtained, while the relaxation rate that is concerned with the lifetime of the persistent current and is an important engineering quantity can be obtained. In principle it is possible to obtain a value closer to the true pinning potential energy by inducing a current at slightly higher temperature and then measuring the relaxation of that current at some chosen lower temperature. However, if we wish to get a more exact value, an astronomically long time will be needed for the measurements.

When flux creep becomes pronounced at high temperatures, the flux motion occurs frequently, resulting in a steady electric field even for a small transport current. That is, the critical current density J_c is zero. In this regime magnetic hysteresis does not appear under a quasistatic variation of the applied field; i.e., the magnetization is reversible. The boundary between the reversible region with $J_c = 0$ and the irreversible one with $J_c \neq 0$ on the temperature vs. magnetic field plane is called the irreversibility line (see Fig. 3.50). Figure 3.51 is a set of magnetization curves for Pb-In [46]. It can be seen that the magnetization becomes reversible at high magnetic fields in specimens with weak pinning forces, and that the reversible region shrinks with increasing pinning strength. This shows that the irreversibility line depends on the pinning strength. At higher temperatures flux creep is stronger and hence, the above features are more noticeable in high-temperature superconductors. The melting of flux line lattice, the vortex glass-liquid transition, etc., were also proposed as for the origin of the irreversibility line. In this book we follow the mechanism of the flux creep. The detailed discussion on this point for high-temperature superconductors will be given in Sect. 8.2.

The irreversibility line at a given temperature T is defined as the magnetic field, $H_i(T)$, at which the critical current density determined in terms of the electric field criterion, $E = E_c$, for example, reduces to zero. That is, neglecting the second term in (3.116) again, from the requirement that $U = U_0$ in the limit $J = J_c = 0$ we have

$$U_0(H_i) = k_B T \log\left(\frac{\mu_0 H_i a_f \nu_0}{E_c}\right). \tag{3.130}$$

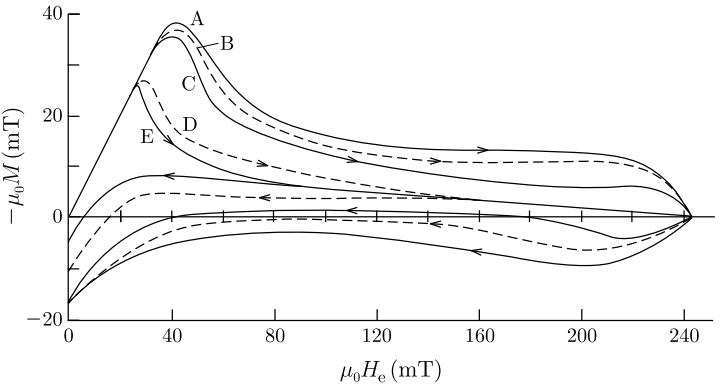

Fig. 3.51 Magnetization curves for Pb-8.23wt%In specimens with various flux pinning strengths [46]. 'A' is a specimen after cold working and 'B', 'C', 'D' and 'E' are specimens annealed at room temperature for 30 min., 1 day, 18 days and 46 days, respectively

As expected, U_0 depends on the flux pinning strength and is a function of magnetic field and temperature. Hence, the irreversibility line, $H_\mathrm{i}(T)$, can be obtained from (3.130). The estimation of U_0 will take place in Sect. 7.7, and examples of the irreversibility line for high-temperature superconductors will be shown in Sect. 8.5. It was mentioned above that only the apparent pinning potential energy U_0^* can be obtained from the measurement of magnetic relaxation. On the other hand, the irreversibility line is directly related to the true pinning potential energy U_0. Hence, U_0 can be estimated from a measured value of the irreversibility field.

At higher temperatures and/or higher magnetic fields the flux lines tend to creep in the direction of the Lorentz force and a voltage appears. This mechanism is identical with that of flux flow. Based on this concept the voltage states in Fig. 3.44(a) and (c) are the creep state and the flow state, respectively. However, these are not easily discerned experimentally. In the regime of flux creep, we make the approximation

$$U' \simeq U + f a_\mathrm{f} = U + \pi U_0 \frac{J}{J_{\mathrm{c}0}} \tag{3.131}$$

for use in (3.116). If the second term is sufficiently less than $k_\mathrm{B} T$, the

$$E \simeq \frac{\pi B a_\mathrm{f} \nu_0 U_0 J}{J_{\mathrm{c}0} k_\mathrm{B} T} \exp\left(-\frac{U_0}{k_\mathrm{B} T}\right). \tag{3.132}$$

This is an ohmic current-voltage characteristic, which takes into consideration the fact that U approaches U_0 in the range of sufficiently small J. This is called Thermally Assisted Flux Flow (TAFF). The corresponding electric resistivity is obtained as

$$\rho = \rho_0 \exp\left(-\frac{U_0}{k_\mathrm{B} T}\right), \tag{3.133}$$

where $\rho_0 = \pi B a_f \nu_0 U_0 / J_{c0} k_B T$ can be approximately regarded as a constant within a narrow temperature range. This suggests that U_0 may be estimated from the slope of the log ρ vs. $1/T$. However, as pointed out by Yeshurun and Malozemoff [47], such an attempt would lead to error, since U_0 varies with temperature. If we write $U_0 = K(1 - T/T_c)^p$, for instance, at high temperatures, it is easy to derive

$$\frac{\partial \log \rho}{\partial (1/T)} = -\frac{U_0}{k_B}\left(1 + \frac{pT}{T_c - T}\right). \tag{3.134}$$

This suggests that a simple plot of $\log \rho$ vs. $1/T$ would lead to an overestimate of U_0, especially so in the vicinity of T_c. Generally the value of p is unknown and U_0 cannot be obtained. This is due to the fact that (3.133) is correct in a fixed magnetic field only within a very narrow temperature range. It is possible to observe an electric resistivity similar to that of (3.133) in the presence of a large transport current. In this case the condition of Fig. 3.48(a) holds and what is obtained is none other than U_0^*. The apparent pinning potential energy obtained in this method agrees well with that obtained from magnetic relaxation [48].

A very wide reversible region exists between the irreversibility line, $H_i(T)$, and the phase boundary, $H_{c2}(T)$, as shown in Fig. 3.50 for a superconductor with a weak pinning force; this leads to a wide resistive transition. Hence, it is claimed that the width of the resistive transition is determined by the pinning strength. When

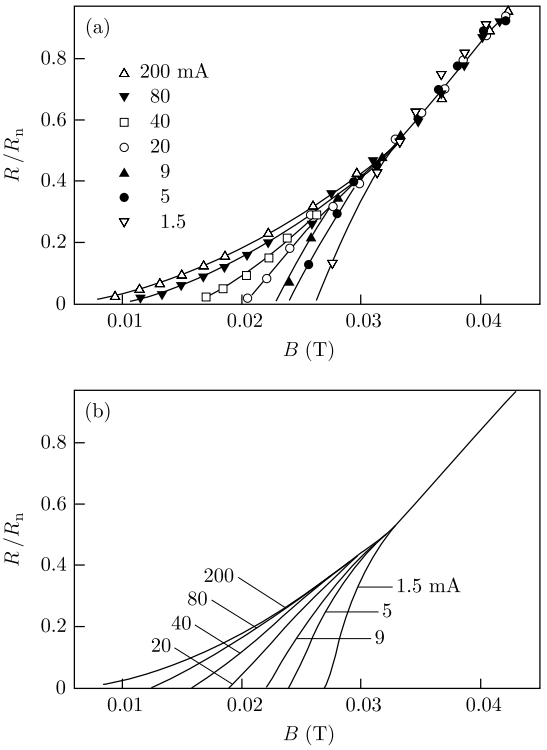

Fig. 3.52 (**a**) Resistance vs. magnetic field at 4.2 K for a Nb-Ta specimen with weak pinning force [28]. (**b**) Theoretically calculated resistance vs. magnetic field assuming a flux flow with observed critical current density and flux flow resistivity [49]

the temperature is lowered slightly below the irreversibility line, J_c recovers suddenly. On the other hand, if the temperature is slightly increased, a variation from the flux creep state to the flux flow state takes place. Hence, the flux lines are considered to be in the flow state throughout most of the wide resistive transition. Figure 3.52(a) shows the broad magnetic field range of the resistive transition that has been measured for a Nb-Ta alloy [28] under various current densities; (b) shows the corresponding theoretical results [49] constructed from the observed critical current density and flux flow resistivity. These agree well with each other in the range where a small resistivity due to the flux creep can be disregarded. This supports the speculation that the dominant component of the usually observed resistive transition comes from flux flow. Such a broad resistive transition is also observed for high-temperature superconductors and the same discussion can be repeated in principle. However, the effect of flux creep is then much more noticeable and the region of low resistivity will be further widened. In addition the effect of the superconducting fluctuations is considered to be large around the phase boundary and the shape of the resistive transition itself seems to be strongly influenced by the fluctuations.

3.9 Exercises

3.1. Derive (3.18), (3.19) and (3.20).
3.2. Derive the viscous energy loss density given by the second term of (3.33) directly from the second term of (2.73). (*Hint*: Since the viscous energy loss density is small, (3.28), the quasistatic value for the velocity of flux lines, can be used.)
3.3. Using the method of (2.74), derive (3.40), the energy loss density when an AC magnetic field is applied to a current-carrying superconductor.
3.4. Derive (3.60) from (3.59).
3.5. Calculate the DC susceptibility in the field cooled process when the parameter m' in (3.80), representing the temperature dependence of J_c, is equal to 2.
3.6. Calculate the DC susceptibility when a constant magnetic field is applied and then, the temperature is elevated after cooling down at zero field.
3.7. From the area of the $\langle B \rangle$-H loop, derive (3.110), the AC energy loss density in a superconducting slab thinner than the AC penetration depth λ_0', in a parallel AC magnetic field.
3.8. Derive η_p in Fig. 3.38 for a bulk superconductor for a sufficiently small AC field amplitude h_0 using the Campbell model.
3.9. Derive (3.112), where the superconductor is a slab of thickness d_f.
3.10. Prove that the half size of a superconductor must be smaller than the AC penetration depth, λ_0', for the effect of reversible flux motion to be significant. For simplicity it is assumed that the AC magnetic field is applied parallel to a wide superconducting slab of thickness $2d$. (*Hint*: Use the condition that the maximum displacement of flux lines in the superconductor in one period is less than the diameter of the pinning potential, $2d_i$.)

3.11. The current density dependence of the energy barrier, U, is assumed as $U(J) = U_0(1 - J/J_{c0})^N$, where $N > 1$. Discuss the dependences of the apparent pinning potential energy, U_0^*, on the temperature, T, and U_0, using Fig. 3.45.

3.12. When the resistivity criterion, $\rho = \rho_c$, is used for the definition of the critical current density, how is the expression of the irreversibility line different from (3.130)? (*Hint*: Use (3.132)).

References

1. F. Irie, K. Yamafuji, J. Phys. Soc. Jpn. **23**, 255 (1967)
2. R. Hancox, Proc. IEEE **113**, 1221 (1966)
3. T. Matsushita, F. Sumiyoshi, M. Takeo, F. Irie, Technol. Rep. Kyushu Univ. **51**, 47 (1978) [in Japanese]
4. W.T. Norris, J. Phys. D, Appl. Phys. **3**, 489 (1970)
5. C.P. Bean, Phys. Rev. Lett. **8**, 250 (1962)
6. H. London, Phys. Lett. **6**, 162 (1963)
7. M. Askin, J. Appl. Phys. **50**, 7060 (1979)
8. V.B. Zenkevitch, V.V. Zheltov, A.S. Romanyuk, Sov. Phys. Dokl. **25**, 210 (1980)
9. C.Y. Pang, A.M. Campbell, P.G. McLaren, IEEE Trans. Magn. **17**, 134 (1981)
10. Y. Kato, M. Noda, K. Yamafuji, Technol. Rep. Kyushu Univ. **53**, 357 (1980) [in Japanese]
11. M. Noda, K. Funaki, K. Yamafuji, Mem. Fac. Eng., Kyushu Univ. **46**, 63 (1986)
12. M. Noda, K. Funaki, K. Yamafuji, Technol. Rep. Kyushu Univ. **58**, 533 (1985) [in Japanese]
13. E.H. Brandt, M.V. Indenbom, A. Forkl, Europhys. Lett. **22**, 735 (1993)
14. T. Kawashima, T. Sueyoshi, K. Yamafuji, Jpn. J. Appl. Phys. **17**, 699 (1978)
15. K. Kaiho, K. Koyama, I. Todoroki, Cryog. Eng. Jpn. **5**, 242 (1970) [in Japanese]
16. N. Sakamoto, K. Yamafuji, Jpn. J. Appl. Phys. **16**, 1663 (1977)
17. T. Ogasawara, Y. Takahashi, K. Kambara, Y. Kubota, K. Yasohama, K. Yasukochi, Cryogenics **19**, 736 (1979)
18. F. Rothwarf, C.T. Rao, L.W. Dubeck, Solid State Commun. **11**, 1123 (1972)
19. K. Funaki, K. Yamafuji, Jpn. J. Appl. Phys. **21**, 299 (1982)
20. K. Funaki, T. Nidome, K. Yamafuji, Jpn. J. Appl. Phys. **21**, 1121 (1982)
21. K. Funaki, M. Noda, K. Yamafuji, Jpn. J. Appl. Phys. **21**, 1580 (1982)
22. H.T. Coffey, Cryogenics **7**, 73 (1967)
23. K. Yamafuji, M. Takeo, J. Chikaba, N. Yano, F. Irie, J. Phys. Soc. Jpn. **26**, 315 (1969)
24. H.J. Fink, Phys. Lett. **19**, 364 (1965)
25. C.P. Bean, J.D. Livingston, Phys. Rev. Lett. **12**, 14 (1964)
26. P.G. de Gennes, *Superconductivity of Metals and Alloys* (Benjamin, New York, 1966) (Translated by P.A. Pincus). Sect. 3.2
27. P.G. de Gennes, Solid State Commun. **3**, 127 (1965)
28. R.A. French, J. Lowell, K. Mendelssohn, Cryogenics **7**, 83 (1967)
29. H.R. Hart Jr., P.S. Swartz, Phys. Rev. **156**, 403 (1967)
30. T. Matsushita, T. Honda, Y. Hasegawa, Y. Monju, J. Appl. Phys. **54**, 6526 (1983)
31. T. Matsushita, T. Honda, K. Yamafuji, Mem. Fac. Eng., Kyushu Univ. **43**, 233 (1983)
32. L.J. Barnes, H.J. Fink, Phys. Lett. **20**, 583 (1966)
33. S.T. Sekula, R.H. Kernohan, Phys. Rev. B **5**, 904 (1972)
34. T. Matsushita, E.S. Otabe, T. Matsuno, M. Murakami, K. Kitazawa, Physica C **170**, 375 (1990)
35. A.M. Campbell, J. Phys. C **4**, 3186 (1971)
36. T. Matsushita, N. Harada, K. Yamafuji, M. Noda, Jpn. J. Appl. Phys. **28**, 356 (1989)

37. F. Sumiyoshi, M. Matsuyama, M. Noda, T. Matsushita, K. Funaki, M. Iwakuma, K. Yamafuji, Jpn. J. Appl. Phys. **25**, L148 (1986)
38. S. Takács, A.M. Campbell, Supercond. Sci. Technol. **1**, 53 (1988)
39. P.W. Anderson, Y.B. Kim, Rev. Mod. Phys. **36**, 39 (1964)
40. K. Yamafuji, T. Fujiyoshi, K. Toko, T. Matsushita, Physica C **159**, 743 (1989)
41. T. Matsushita, E.S. Otabe, Jpn. J. Appl. Phys. **31**, L33 (1992)
42. D.O. Welch, IEEE Trans. Magn. **27**, 1133 (1991)
43. M.R. Beasley, R. Labusch, W.W. Webb, Phys. Rev. **181**, 682 (1969)
44. C.W. Hagen, R. Griessen, Phys. Rev. Lett. **62**, 2857 (1989)
45. M.V. Feigel'man, V.B. Geshkenbein, A.I. Larkin, V.M. Vinokur, Phys. Rev. Lett. **63**, 2303 (1989)
46. J.D. Livingston, Phys. Rev. **129**, 1943 (1963)
47. Y. Yeshurun, A.P. Malozemoff, Phys. Rev. Lett. **60**, 2202 (1988)
48. K. Yamafuji, Y. Mawatari, T. Fujiyoshi, K. Miyahara, K. Watanabe, S. Awaji, N. Kobayashi, Physica C **185–189**, 2285 (1991)
49. T. Matsushita, B. Ni, Physica C **166**, 423 (1990)